https://doi.org/10.5194/egusphere-2025-4543
Preprint. Discussion started: 30 October 2025

GEOS-Chem-hyd: enabling source-oriented sensitivity analysis with GEOS-Chem

Samuel O. Akinjole[1] and Shannon L. Capps[1]

[1]Department of Civil, Architectural & Environmental Engineering, Drexel University, Philadelphia, 19104, PA, USA

Correspondence to: Shannon L. Capps (shannon.capps@drexel.edu)

Abstract. Effective environmental policymaking requires accurate quantification of the impacts on air quality of changes in emissions. Chemical transport models, such as GEOS-Chem, are widely used for such analysis. Traditional methods to compute the relative influence of a change in emissions, or the sensitivity of pollutant concentrations to a change in emissions, with these models often suffer from numerical inaccuracies, especially when evaluating nonlinear atmospheric processes. To overcome these limitations, we integrated a novel sensitivity analysis approach leveraging hyperdual numbers into GEOS-Chem, making GEOS-Chem-hyd. The hyperdual step method accurately calculates first- and second-order sensitivities simultaneously and avoids common numerical errors associated with traditional finite difference methods. The real concentrations as well as first- and second-order sensitivities with respect to emissions calculated with GEOS-Chem-hyd align with the values calculated with GEOS-Chem version 14.0.0 within expected error. Applying GEOS-Chem-hyd to assess how changes in emissions of oxides of nitrogen could be expected to alter ozone, particulate matter, ammonium, and biogenic organic aerosol concentrations demonstrated regional differences and nonlinear influences. As an example of regional variations, the emissions of oxides of nitrogen were shown to decrease biogenic organic aerosol in most areas, except in portions of the boreal forests in Siberia. The nonlinear influence of emissions of oxides of nitrogen on ozone, ammonium, and biogenic organic aerosol was evidenced by second-order sensitivities on the same order of magnitude as the first-order sensitivities. GEOS-Chem-hyd incurs approximately four times greater computational costs than GEOS-Chem, which is competitive with the three GEOS-Chem model executions required for less accurate second-order sensitivities using the central finite difference method. GEOS-Chem-hyd provides a framework for efficient assessment of the influence of new scientific modules, which are easily incorporated into the sensitivity analysis framework, and supports informed emission control policy development through accurate, source-oriented sensitivity analysis.

1 Introduction

Short-lived air pollution remains one of the most pressing global environmental challenges as approximately 7.7% of annual deaths and 4.5% of disability adjusted life-years (DALYs) worldwide were attributable to ambient exposure in 2021 (IHME, 2024). Specifically, exposure to particulate matter less than 2.5 µm in aerodynamic diameter ($PM_{2.5}$) and ozone (O_3) formed from emissions of precursor gases, such as oxides of nitrogen (NO_x), or primary particulates has been associated with morbidity and premature mortality (Brauer et al., 2012; Burnett et al., 2014). Addressing such significant public health concerns requires understanding the nonlinear atmospheric processes that govern pollutant formation and transport. Chemical transport models (CTMs) have proven valuable to scientists and environmental decisionmakers for estimating pollutant concentrations. CTMs solve time-dependent, coupled partial differential equations representing the motion and chemical transformations of pollutants based on meteorological inputs and emissions estimates. Several CTMs have proven purposeful for understanding nonlinear atmospheric chemistry (Carter et al., 2021; Field et al., 2016; Kharol et al., 2013; Le et al., 2020; Keller et al., 2021; Pai et al., 2021; Schiferl et al., 2014; Shrivastava et al., 2017), improving estimates of emissions (Chen et al., 2021; Fu et al., 2022; Henze et al., 2009; Mao

https://doi.org/10.5194/egusphere-2025-4543
Preprint. Discussion started: 30 October 2025

et al., 2015; Moon et al., 2024; Qu et al., 2017; Sitwell et al., 2022; Van Der Graaf et al., 2022; Zhang et al., 2016; Zhang et al., 2020; Zhu et al., 2015), and developing efficient emissions control strategies (Anenberg et al., 2019; Capps et al., 2010; Ding et al., 2019; Lyu et al., 2021; Pusede et al., 2016; Tian et al., 2010; Tsimpidi et al., 2007; Turner et al., 2015; Wang et al., 2005; Yang and Zhao, 2023; Zhao et al., 2022). GEOS-Chem is a widely-used, three-dimensional (3D) global CTM representing the multiphase chemistry of the troposphere and stratosphere (Bey et al., 2001).

Sensitivity analysis in CTMs quantifies how changes in input variables, such as the emissions of select species, affect output variables, such as species concentrations. CTMs involve time-dependent, coupled partial differential equations and numerical solvers (Seinfeld and Pandis, 2016), which makes quantifying these influences accurately challenging. Accordingly, several approaches to sensitivity analysis have been developed with select implementations in various CTMs. Forward sensitivities reflect the influence of select model parameters or sources on all modelled results or concentrations. Examples of approaches that provide forward sensitivities are the finite difference method derived from Taylor's theorem, the complex and multicomplex step method (Lantoine et al., 2012; Martins et al., 2003; Squire and Trapp, 1998), dual and hyperdual step methods (Fike and Alonso, 2011), and tangent linear models (Vukicevic and Errico, 1993; Dunker et al., 2002). Reverse sensitivities reflect the influence on a select receptor of all sources, which is possible through the adjoint method (Errico, 1997). Each method provides a first-order sensitivity and is theoretically extensible to higher orders although complications in development or computational costs are entailed in obtaining accurate higher-order sensitivities. Finally, an alternative approach is tagging parameters, which has been implemented for emissions of relatively non-reactive species (e.g., Fisher et al., 2017; Ikeda et al., 2017; Kim et al., 2015) and for geographically-tagged O_3 tracers (e.g., Cheng et al., 2018; Han et al., 2019; Wang et al., 2011; Whaley et al., 2015). Since this approach yields information valuable for source apportionment yet distinct from the derivatives of other sensitivity analysis approaches, implementations of tagging will not be further addressed.

Of the forward sensitivity analysis approaches, the finite difference method has been applied to GEOS-Chem most extensively. Finite difference methods are the most straightforward to implement because no model development is required, only additional computational cost. First- and second-order sensitivities are calculable based on the Taylor series expansion with two or three model executions, respectively, for the central finite difference. Primarily, the finite difference approach is used to evaluate the impact of a new science module (e.g., Croft et al., 2014; Johnson et al., 2016; Vinken et al., 2011; Sun et al., 2022; Yan et al., 2019). The finite difference-based sensitivities have also been applied in mass balance inversions to improve emissions of select species based on satellite observations (Choi et al., 2022; Cooper et al., 2017; Li et al., 2019). Additionally, the finite difference method is used to evaluate models instrumented to conduct sensitivity analysis (Constantin and Barrett, 2014; Dunker et al., 2002; Henze et al., 2007; Koo et al., 2007). One challenge for these applications is that the finite difference method is prone to truncation and subtractive cancellation errors. The truncation error arises from the neglected higher-order terms with the order of the error being the square of the perturbation size, h, for first- and second-order central finite differences with the minimum number of model executions. To reduce the truncation error, h is minimized; however, the subtractive cancellation error becomes dominant when reducing h leads to the modelled concentrations changes being smaller than the model noise (Constantin and Barrett, 2014; Hakami et al., 2004). In a CTM, the optimal perturbation size varies with the model parameter and output of interest, especially in second-order sensitivities, which makes the finite difference unreliable for computing exact sensitivities (Berman et al., 2023; Liu et al., 2024). Furthermore, changing a source parameter will change the model state, which may be undesirable if the marginal change at the model state is desired. Prior to this work, the only other forward sensitivity analysis technique implemented in GEOS-Chem was the complex step method (Constantin and Barrett, 2014), which was applied to the adjoint of GEOS-Chem and so will be discussed following the adjoint.

https://doi.org/10.5194/egusphere-2025-4543
Preprint. Discussion started: 30 October 2025

Henze et al. (2007) developed the GEOS-Chem adjoint model, which calculates receptor-oriented sensitivities of a concentration-based cost function. This instrumented model is usually formulated by appending to the model the inverted call graph of the model with the transpose of the tangent linear model of each line of code inserted (Giering and Kaminski, 1998). This adjoint development approach is known as the discrete approach, and it follows the numerical solution of the original model. Since the model development method follows rules understandable by machines, efforts to implement automatic differentiation tools proliferated in the early 2000s (e.g., Alexe and Sandu, 2009; Hascoët and Dauvergne, 2008; Heimbach et al., 2005; Utke et al., 2008). An alternative approach is to derive the analytical derivative and implement the transpose of the analytical derivative, which is known as the continuous method and is sometimes a more stable solution (Giles and Pierce, 2000). The GEOS-Chem adjoint has proven tremendously valuable for environmental decisionmakers because the cost functions for which sensitivities are calculated may be location-specific, such as a combined statistical area to be regulated (Lyu et al., 2021); threshold-specific, such as a theoretical limit for health effects (Lapina et al., 2014); or a combination of functions of different species or metrics (Lyu et al., 2019). Furthermore, scientists have leveraged this augmented model to conduct inverse modelling of emissions estimates using observations of air pollutants from satellites (Chen et al., 2021; Choi et al., 2022; Cooper et al., 2017; Elbern et al., 2010; Li et al., 2019; Moon et al., 2024; Park et al., 2016; Qu et al., 2017).

Constantin and Barrett (2014) implemented the complex step method in the GEOS-Chem adjoint, GEOS-Chem XPLEX. Like the finite difference method, the complex step method is derived from the Taylor series expansion. Unlike the finite difference method, the perturbation is propagated in imaginary space, which requires no subtraction, thus, eliminating the cancellation error associated with tiny step sizes. To a more limited degree, truncation errors still exist because the third and higher-order terms are ignored from the Taylor series expansion, which can be minimized by choosing a very small step size (e.g., $O(10^{-20})$). To calculate exact second-order derivatives, the multicomplex method developed by Lantoine et al. (2012) is required, which was not implemented by Constantin and Barrett (2014). However, GEOS-Chem XPLEX allows for the computation of a combination of forward and reverse sensitivities. Unfortunately, this method is computationally intensive and limited in scope to the code for which an adjoint exists (Constantin and Barrett, 2014). A tangent linear model, such as the decoupled direct method (Napelenok et al., 2006), has not been implemented in GEOS-Chem.

Second-order derivatives have proven to be quite useful in sensitivity analysis as they improve the accuracy of the Taylor expansion and allow nonlinear influences of parameters to be quantified, such as those observed in the formation of secondary aerosols or the impact of aviation NO_x emissions on $PM_{2.5}$ concentrations (Constantin and Barrett, 2014). Additionally, inverse modelling may be improved with the availability of the Hessian in addition to the Jacobian as proposed by Bousserez and Henze (2018).

This paper implements the hyperdual step method (Fike and Alonso, 2011), an operator overloading approach for calculating first- and second-order sensitivities, in GEOS-Chem. The method accurately computes source-oriented first- and second-order sensitivities, which aid in quantifying nonlinear relationships. For example, the non-linearities in secondary aerosol formation can be evaluated by calculating the first- and second-order sensitivities (Liu et al., 2024). Like the complex step method, the hyperdual step method arises from the Taylor series expansion yet in dual and hyperdual space such that the outcome is not subject to subtractive cancellation or truncation errors due to the unique properties of hyperdual numbers (Fike and Alonso, 2011). Liu et al. (2024) developed a Fortran library for overloading operators with hyperdual numbers, HDMod (https://github.com/atmmod/HDMod), by translating the C-based library of Fike and Alonso (2011). This operator overloading approach was applied in the Community Multiscale Air Quality model (CMAQ) as the first application of hyperdual numbers in an atmospheric CTM (Liu et al., 2024).

https://doi.org/10.5194/egusphere-2025-4543
Preprint. Discussion started: 30 October 2025

Here, the GEOS-Chem model is augmented with the hyperdual step method to create GEOS-Chem-hyd. In Section 2, we describe hyperdual numbers, their implementation in GEOS-Chem, and the method for evaluating GEOS-Chem-hyd. In Sections 3.1-2, we evaluate the accuracy and computational cost of GEOS-Chem-hyd. In Section 3.3, we demonstrate the usefulness of GEOS-Chem-hyd by evaluating O_3 formation in response to perturbations in total NO_x and isoprene (ISOP) emissions over a week-long simulation. To the best of our knowledge, this is the first augmentation of GEOS-Chem that accurately computes both first- and second-order sensitivities of concentrations with respect to select emissions.

2 Methods

2.1 Hyperdual numbers

Fike and Alonso (2011) introduced hyperdual numbers to compute numerically exact first- and second-order derivatives simultaneously. A hyperdual number, H, is defined as:

$$H = a_0 + a_1\epsilon_1 + a_2\epsilon_2 + a_{12}\epsilon_{12} \tag{1}$$

where, a_0, a_1, a_2, and a_{12} are real number coefficients, and ϵ_1, ϵ_2, and ϵ_{12} are non-real components analogous to the imaginary component, i, of a complex number. These non-real components follow these rules:

$$\epsilon_1^2 = \epsilon_2^2 = \epsilon_{12}^2 = 0 \tag{2}$$

$$\epsilon_1 \neq \epsilon_2 \neq \epsilon_{12} \neq 0 \tag{3}$$

$$\epsilon_1\epsilon_2 = \epsilon_2\epsilon_1 = \epsilon_{12} \tag{4}$$

The square of each non-real component equals zero (Eq. 2). However, these components themselves are not equal to zero (Eq. 3). Multiplication of non-real components is commutative (Eq. 4), while multiplying ϵ_1 and ϵ_2 equals the third non-real component ϵ_{12} (Eq. 4). Hyperdual arithmetic leverages these properties to precisely calculate derivatives using Taylor series expansions (Fike and Alonso, 2011; Liu et al., 2024). Perturbations are either additive or multiplicative, as with finite difference methods. We use only multiplicative perturbations. To perturb a scalar function, $f(x)$, multiplicatively, we multiply x by a hyperdual number, $H_a = 1 + a_1\epsilon_1 + a_2\epsilon_2$. Expanding $f(xH_a)$ yields a Taylor series:

$$\begin{aligned} f(xH_a) = f(x) &+ (xa_1\epsilon_1 + xa_2\epsilon_2)f'(x) \\ &+ \frac{1}{2!}(xa_1\epsilon_1 + xa_2\epsilon_2)^2 f''(x) \\ &+ \frac{1}{3!}(xa_1\epsilon_1 + xa_2\epsilon_2)^3 f'''(x) + \cdots. \end{aligned} \tag{5}$$

Applying hyperdual properties (Eqs. 2-4) simplifies Eq. 5 to

$$\begin{aligned} f(xH_a) = f(x) &+ (xa_1\epsilon_1 + xa_2\epsilon_2)f'(x) \\ &+ x^2 a_1 a_2 \epsilon_{12} f''(x) \end{aligned} \tag{6}$$

where $f(xH_a)$ is a hyperdual number, and the other terms in Eq. 5 are zero due to the properties of hyperdual numbers. Rearranging and extracting the non-real components of the left-hand side and right-hand side of Eq. 6, provides numerically exact derivatives:

$$f'(x) = \frac{\epsilon_1 part[f(xH_a)]}{xa_1} = \frac{\epsilon_2 part[f(xH_a)]}{xa_2} \tag{7}$$

$$f''(x) = \frac{\epsilon_{12} part[f(xH_a)]}{x^2 a_1 a_2} \tag{8}$$

where the notation $\epsilon_1 part[]$, $\epsilon_2 part[]$, and $\epsilon_{12} part[]$ represents the extraction of coefficients associated with ϵ_1, ϵ_2, and ϵ_{12}, respectively. The extracted coefficients are the a_1, a_2, and a_{12} components of the function evaluation. Unlike the finite difference method, these expressions do not involve numerical subtraction or truncation of higher-order terms. Therefore, hyperdual

https://doi.org/10.5194/egusphere-2025-4543
Preprint. Discussion started: 30 October 2025

arithmetic eliminates common numerical issues like subtractive cancellation and truncation errors. This method is extensible to vector-valued functions, $f(x)$, where $x = [x_1, x_2, \dots, x_n]$. Perturbing a single variable, x_1, yields first and second derivatives with respect to x_1 as shown:

$$\frac{\partial f(x)}{\partial x_1} = \frac{\epsilon_1 part\left[f\left(xH_{a,x_1}\right)\right]}{x_1 a_1} = \frac{\epsilon_2 part\left[f\left(xH_{a,x_1}\right)\right]}{x_1 a_2} \tag{9}$$

$$\frac{\partial^2 f(x)}{\partial x_1^2} = \frac{\epsilon_{12} part\left[f\left(xH_{a,x_1}\right)\right]}{{x_1}^2 a_1 a_2} \tag{10}$$

Additionally, hyperdual arithmetic allows for simultaneous perturbation of multiple variables, facilitating efficient cross-sensitivity computation. Perturbing two independent variables, x_1 and x_2, yields the following derivatives:

$$\frac{\partial f(x)}{\partial x_1} = \frac{\epsilon_1 part[f(xH_a)]}{x_1 a_1} \tag{11}$$

$$\frac{\partial f(x)}{\partial x_2} = \frac{\epsilon_2 part[f(xH_a)]}{x_2 a_2} \tag{12}$$

$$\frac{\partial^2 f(x)}{\partial x_1\, \partial x_2} = \frac{\epsilon_{12} part[f(xH_a)]}{x_1 x_2 a_1 a_2} \tag{13}$$

where the first-order sensitivities of each independent variable are given by Eqs. 11-12 and the cross-sensitivity in Eq. 13. This versatility makes the hyperdual step method particularly suitable for evaluating sensitivities in computationally demanding and highly nonlinear systems, such as CTMs.

2.2 GEOS-Chem Implementation of the hyperdual step method

GEOS-Chem simulates concentrations by solving the generalized continuity equation for an Eulerian 3-D grid (Seinfeld and Pandis, 2016; Zhang et al., 2012):

$$\frac{\partial C_i}{\partial t} = -\nabla \cdot (\boldsymbol{u} C_i) + \nabla \cdot (\boldsymbol{K} \nabla C_i) + R_i(C_1, C_2, \dots, C_n) + E_i - S_i \tag{14}$$

where C_i is the concentration of species i, $\boldsymbol{u}$ is the wind velocity vector, $\boldsymbol{K}$ is the turbulent diffusivity, R_i is the chemical production rate for species i, E_i is the emission rate for species i, and S_i is the removal flux for species i. Here, the hyperdual step method is implemented in GEOS-Chem version 14.0.0.rc-2 + revert pressure fixer. The model is executed at 4˚ x 5˚ spatial resolution with 72 vertical layers. MERRA-2 meteorological fields (Gelaro et al., 2017) and global anthropogenic emissions from the CEDS v2 inventory (O'rourke et al., 2021) are used as inputs, with the configuration settings available at https://doi.org/10.5281/zenodo.16575028. The GEOS-Chem model utilizes the KPP mechanism (Sandu and Sander, 2006) for gas-phase chemistry and the forward mode of ISORROPIA for aerosol thermodynamics (Fountoukis and Nenes, 2007; Pye et al., 2009). Dry deposition utilizes a standard resistance-in-series scheme (Wesely, 1989) with several modifications (Jaeglé et al., 2018; Wang et al., 1998), and wet deposition follows a developed scheme (Jacob et al., 2000) that includes washout and rainout of soluble species (Liu et al., 2001). Transport follows the TPCORE advection scheme (Lin and Rood, 1996), while the non-local PBL mixing scheme is used (Lin and Mcelroy, 2010). For all the simulations used here, the timesteps were 20-min for chemistry and 10-min for transport (Philip et al., 2016).

The hypderdual version of GEOS-Chem, GEOS-Chem-hyd, enables the application of the hyperdual step method. The appropriate variables are converted to hyperdual numbers, which requires an operator overloading library (Fike and Alonso, 2011). For GEOS-Chem-hyd, we employ the HDMod Fortran library developed by Liu et al. (2024), which was further developed to support additional array operations specific to the GEOS-Chem source code. Implementation of the hyperdual step method entails changing the type to hyperdual of selected variables in the routines that influence selected output concentrations. The corresponding

https://doi.org/10.5194/egusphere-2025-4543
Preprint. Discussion started: 30 October 2025

derivatives are inherently evaluated through every overloaded operation as the first-order derivative information is held in the ϵ_1 and ϵ_2 components while the second-order derivative information is contained in the ϵ_{12} component. Additional diagnostics were added to obtain the non-real components for species concentrations and aerosol mass using the same structure as those of the real components.

GEOS-Chem has several modules that are sufficiently complicated to require independent development and evaluation. For instance, the inorganic aerosol thermodynamics are calculated using ISORROPIA, which has thousands of lines of Fortran, so a standalone version of ISORROPIA developed for testing for GEOS-Chem (Berman et al., 2023) was employed to evaluate the accuracy of the sensitivities of this hyperdualized module independently of other GEOS-Chem-hyd code. Similarly, the chemistry and aerosol modules were unit tested. The Harmonized Emissions Component (HEMCO) is a standalone model for emissions (Lin et al., 2021). For the purposes of introducing GEOS-Chem-hyd, the emission routines that interface with GEOS-Chem Classic are made hyperdual.

The computational cost for a hyperdual calculation ranges from 4 to 14 times that of a real number calculation (Fike and Alonso, 2011). Although all real variables in GEOS-Chem could have been converted to hyperdual type, as in GEOS-Chem-XPLEX (Constantin and Barrett, 2014), we reduced the computational cost by selectively converting the necessary variables. Specifically, the species concentration array and all other variables that depend on or influence the species concentration array across GEOS-Chem were changed to the hyperdual type (Figure 1).

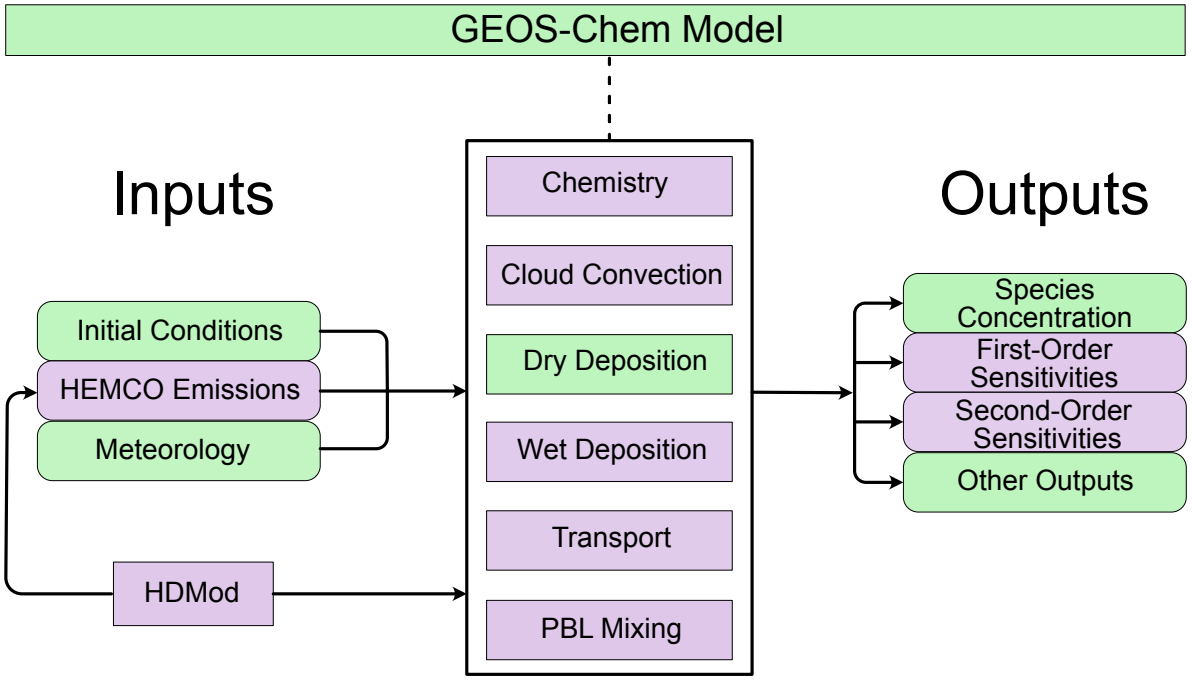

Figure 1: A schematic of the GEOS-Chem-hyd model. Purple components highlight modifications to the standard model for hyperdual calculations, utilizing the overloading library, HDMod. First- and second-order sensitivities are calculable from new outputs of hyperdual calculations.

2.3 Evaluating sensitivities from GEOS-Chem-hyd

The implementation of a novel sensitivity analysis technique in a model requires evaluation to ensure that the behaviour of the underlying model is represented accurately in the augmented model (Hakami et al., 2004; Napelenok et al., 2006; Zhang et al., 2012). Here, comparisons of the first-order sensitivities from the hyperdual step method are made with those of the central

https://doi.org/10.5194/egusphere-2025-4543
Preprint. Discussion started: 30 October 2025

finite difference method and of the second-order sensitivities with a hybrid central finite difference approach. Semi-normalized sensitivities, which reflect a change in concentration in the numerator corresponding to a fractional change in the concentration or emissions in the denominator, are of use in both emissions control strategy development and in data assimilation. We apply multiplicative perturbations in the dual space in GEOS-Chem-hyd to produce semi-normalized sensitivities without the need for post-processing with additional information about the denominator.

To illustrate, the first-order semi-normalized sensitivity of O_3 concentrations at the ground layer, $C_{O_3,i,j,l=0,t}$, for a time-averaged simulation to a persistent NO_x emission, $E_{NO_x,i,j,l,t}$, perturbation using the central finite difference method is given by

$$\frac{\partial \overline{C_{O_3,i,j,l=0,t}}\big|_t}{\partial E_{NO_x,i,j,l,t}} \sum_{t=0}^{t_f} E^{def}_{NO_x,i,j,l,t} \approx \frac{\overline{C^{inc}_{O_3,i,j,l=0,t}}\Big|_t - \overline{C^{dec}_{O_3,i,j,l=0,t}}\Big|_t}{\sum_{t=0}^{t_f} E^{inc}_{NO_x,i,j,l,t} - \sum_{t=0}^{t_f} E^{dec}_{NO_x,i,j,l,t}} \sum_{t=0}^{t_f} E^{def}_{NO_x,i,j,l,t} \tag{15}$$

where subscripts i, j, and l are the longitudinal, latitudinal, and vertical indices for the grid cell; t is the timestep from the start of the model simulation; t_f is the final timestep of the model simulation; the superscript inc indicates a positive perturbation in real space; the superscript dec indicates a negative perturbation in real space; and the superscript def indicates that no real perturbation was applied. Another advantage of semi-normalized sensitivities is that the sum of the emissions over the episode is not required to calculate semi-normalized sensitivities as

$$\frac{\partial \overline{C_{O_3,i,j,l=0,t}}\big|_t}{\partial E_{NO_x,i,j,l,t}} \sum_{t=0}^{t_f} E^{def}_{NO_x,i,j,l,t} \approx \frac{\overline{C^{inc}_{O_3,i,j,l=0,t}}\Big|_t - \overline{C^{dec}_{O_3,i,j,l=0,t}}\Big|_t}{2p} \tag{16}$$

where p is the magnitude of the multiplicative perturbation. Unless stated otherwise, the perturbation sizes used in this manuscript are $\pm 5\%$ for the finite difference domain-wide emissions (p= 0.05). We found this perturbation size to be large enough to observe beyond numerical noise while still small enough to represent local emission changes for the evaluation. These semi-normalized sensitivities have the unit of parts per billion for the species concentration collection and micrograms per meter cubed for the aerosol mass collection.

The first-order semi-normalized sensitivity of time-averaged, ground-level O_3 concentrations to NO_x emissions is calculated with a multiplicative hyperdual perturbation, $H_a = 1.0 + a_1\epsilon_1 + a_2\epsilon_2$, using the hyperdual step method as

$$\frac{\partial \overline{C_{O_3,i,j,l=0,t}}\big|_t}{\partial E_{NO_x,i,j,l,t}} \sum_{t=0}^{t_f} E^{def}_{NO_x,i,j,l,t} = \frac{\epsilon_1 part\left[\overline{C^{def}_{C_{O_3},i,j,l,t}}\Big|_t\right]}{a_1 \sum_{t=0}^{t_f} E^{def}_{NO_x,i,j,l,t}} \sum_{t=0}^{t_f} E^{def}_{NO_x,i,j,l,t} = \frac{\epsilon_2 part\left[\overline{C^{def}_{C_{O_3},i,j,l,t}}\Big|_t\right]}{a_2 \sum_{t=0}^{t_f} E^{def}_{NO_x,i,j,l,t}} \sum_{t=0}^{t_f} E^{def}_{NO_x,i,j,l,t} \tag{17}$$

where the persistent perturbation in ϵ_1 space is a_1 and ϵ_2 space is a_2. This expression can be further simplified to

$$\frac{\partial \overline{C_{O_3,i,j,l=0,t}}\big|_t}{\partial E_{NO_x,i,j,l,t}} \sum_{t=0}^{t_f} E^{def}_{NO_x,i,j,l,t} = \frac{\epsilon_1 part\left[\overline{C^{def}_{C_{O_3},i,j,l,t}}\Big|_t\right]}{a_1} = \frac{\epsilon_2 part\left[\overline{C^{def}_{C_{O_3},i,j,l,t}}\Big|_t\right]}{a_2} \tag{18}$$

where the first-order semi-normalized sensitivity can be obtained from either the ϵ_1 or the ϵ_2 part divided by the respective perturbation in ϵ_1 space (a_1) or ϵ_2 space (a_2).

For the second-order sensitivities, the central finite difference method is second-order accurate. However, if the relationship is nonlinear, the result is highly dependent on perturbation sizes because the altered model states affect the response (Zhang et al., 2012). As such, a hybrid hyperdual-central finite difference (hybrid) method is used (Berman et al., 2023), which reduces the dependence on the model state changing. This method was also utilized to evaluate the implementation of the hyperdual step method in CMAQ (Liu et al., 2024). The second-order semi-normalized sensitivity of the average concentration with respect to a persistent perturbation in emissions using the hybrid method can be expressed as:

https://doi.org/10.5194/egusphere-2025-4543
Preprint. Discussion started: 30 October 2025

$$\frac{\partial^2 \overline{C_{O_3,i,j,l=0,t}}\big|_t}{\partial E^2_{NO_x,i,j,l,t}}\left(\sum_{t=0}^{t_f} E^{def}_{NO_x,i,j,l,t}\right)^2 \approx \frac{\dfrac{\epsilon_2 part\left[\overline{C^{inc}_{O_3,i,j,l,t}}\big|_t\right]}{a_2\sum_{t=0}^{t_f} E^{inc}_{NO_x,i,j,l,t}} - \dfrac{\epsilon_2 part\left[\overline{C^{dec}_{O_3,i,j,l,t}}\big|_t\right]}{b_2\sum_{t=0}^{t_f} E^{dec}_{NO_x,i,j,l,t}}}{\sum_{t=0}^{t_f} E^{inc}_{NO_x,i,j,l,t} - \sum_{t=0}^{t_f} E^{dec}_{NO_x,i,j,l,t}}\left(\sum_{t=0}^{t_f} E^{def}_{NO_x,i,j,l,t}\right)^2 \tag{19}$$

where the *inc* case is perturbed in the real space by 5% and dual spaces by $H_a = 1.0 + a_1\epsilon_1 + a_2\epsilon_2$ and the *dec* case is perturbed in the real space by -5% and dual spaces by $H_b = 1.0 + b_1\epsilon_1 + b_2\epsilon_2$. Depending on the choice of the hyperdual perturbation, the numerator is evaluated from either the ϵ_1 or the ϵ_2 part. The lowest denominator is the perturbation size in the real part, which simplifies as

$$\frac{\partial^2 \overline{C_{O_3,i,j,l=0,t}}\big|_t}{\partial E^2_{NO_x,i,j,l,t}}\left(\sum_{t=0}^{t_f} E^{def}_{NO_x,i,j,l,t}\right)^2 \approx \frac{\epsilon_2 part\left[\overline{C^{inc}_{O_3,i,j,l,t}}\big|_t\right]}{2a_2 p(1+p)} - \frac{\epsilon_2 part\left[\overline{C^{dec}_{O_3,i,j,l,t}}\big|_t\right]}{2b_2 p(1-p)} \tag{20}$$

The simplified hyperdual step method semi-normalized second-order sensitivities can be expressed as

$$\frac{\partial^2 \overline{C_{O_3,i,j,l=0,t}}\big|_t}{\partial E^2_{NO_x,i,j,l,t}}\left(\sum_{t=0}^{t_f} E^{def}_{NO_x,i,j,l,t}\right)^2 = \frac{\epsilon_{12} part\left[\overline{C^{def}_{C_{O_3},i,j,l,t}}\big|_t\right]}{a_1 a_2} \tag{21}$$

In this case, only one simulation is run with a hyperdual perturbation of $H_a = 1.0 + a_1\epsilon_1 + a_2\epsilon_2$, where the emissions in the denominator also cancel out, and the second-order semi-normalized sensitivity is obtained from the ϵ_{12} part divided by the product of the perturbations, $a_1 a_2$.

In addition, cross-sensitivities can be obtained using hybrid and the hyperdual step methods. To illustrate, the semi-normalized cross-sensitivity of ground-level O_3 concentrations at a given time, $C_{O_3,i,j,l=0,t}$, to NO_x and ISOP emissions using the hybrid method is given by

$$\begin{aligned}\frac{\partial^2 \overline{C_{O_3,i,j,l=0,t}}\big|_t}{\partial E_{NO_x,i,j,l,t}\,\partial E_{ISOP,i,j,l,t}}&\left(\sum_{t=0}^{t_f} E^{def}_{NO_x,i,j,l,t}\,E^{def}_{ISOP,i,j,l,t}\right)\\ &\approx \frac{\dfrac{\epsilon_2 part\left[\overline{C^{inc}_{O_3,i,j,l,t}}\big|_t\right]}{a_2\sum_{t=0}^{t_f} E^{def}_{ISOP,i,j,l,t}} - \dfrac{\epsilon_2 part\left[\overline{C^{dec}_{O_3,i,j,l,t}}\big|_t\right]}{b_2\sum_{t=0}^{t_f} E^{def}_{ISOP,i,j,l,t}}}{\sum_{t=0}^{t_f} E^{inc}_{NO_x,i,j,l,t} - \sum_{t=0}^{t_f} E^{dec}_{NO_x,i,j,l,t}}\left(\sum_{t=0}^{t_f} E^{def}_{NO_x,i,j,l,t}\,E^{def}_{ISOP,i,j,l,t}\right)\end{aligned} \tag{22}$$

where the real perturbations are applied to the NO_x emissions, $E_{NO_x,i,j,l,t}$, and the hyperdual perturbations are applied to the ϵ_2 space of the ISOP emission, $E_{ISOP,i,j,l,t}$. Practically, this expression simplifies to

$$\frac{\partial^2 \overline{C_{O_3,i,j,l=0,t}}\big|_t}{\partial E_{NO_x,i,j,l,t}\,\partial E_{ISOP,i,j,l,t}}\left(\sum_{t=0}^{t_f} E^{def}_{NO_x,i,j,l,t}\,E^{def}_{ISOP,i,j,l,t}\right) \approx \frac{\epsilon_2 part\left[\overline{C^{inc}_{O_3,i,j,l,t}}\big|_t\right]}{2a_2 p} - \frac{\epsilon_2 part\left[\overline{C^{dec}_{O_3,i,j,l,t}}\big|_t\right]}{2b_2 p} \tag{23}$$

The simplified semi-normalized cross-sensitivity using the hyperdual step method requires only one simulation with a hyperdual perturbation of NO_x emission in the ϵ_1 space, $H_a = 1 + a_1\epsilon_1$ and ISOP emission in the ϵ_2 space, $H_b = 1 + b_2\epsilon_2$, and is given by

$$\frac{\partial^2 \overline{C_{O_3,i,j,l=0,t}}\big|_t}{\partial E_{NO_x,i,j,l,t}\,\partial E_{ISOP,i,j,l,t}}\left(\sum_{t=0}^{t_f} E^{def}_{NO_x,i,j,l,t}\,E^{def}_{ISOP,i,j,l,t}\right) = \frac{\epsilon_{12} part\left[\overline{C^{def}_{C_{O_3},i,j,l,t}}\big|_t\right]}{a_1 b_2} \tag{24}$$

The first-order, second-order, and cross-sensitivities computed by the hyperdual step method have been shown to be numerically exact for the hyperdualized elements of the model (Fike and Alonso, 2011; Liu et al., 2024).

https://doi.org/10.5194/egusphere-2025-4543
Preprint. Discussion started: 30 October 2025

GEOS-Chem-hyd is evaluated against the hybrid first- or second-order sensitivities. We perturb emissions at every chemistry timestep, which is every 20 minutes (Philip et al., 2016) throughout a 24-hour episode. The first-order semi-normalized sensitivities are represented compactly as exemplified below

$$S_{NO_x}^{O_3} = \frac{\partial \overline{C_{O_3,i,j,l=0,t}}\big|_t}{\partial E_{NO_x,i,j,l,t}} \sum_{t=0}^{72} E_{NO_x,i,j,l,t}^{def} \tag{25}$$

where $S_{NO_x}^{O_3}$ is the first-order semi-normalized sensitivity of first layer or ground level O_3 concentrations to NO_x emissions, and the second-order semi-normalized sensitivity as

$$S_{NO_x}^{(2)O_3} = \frac{\partial^2 \overline{C_{O_3,i,j,l=0,t}}\big|_t}{\partial E_{NO_x,i,j,l,t}^2} \left(\sum_{t=0}^{72} E_{NO_x,i,j,l,t}^{def} \right)^2 \tag{26}$$

where $S_{NO_x}^{(2)O_3}$ is the second-order semi-normalized sensitivity of O_3 concentration to NO_x emissions.

3 Results and Discussion

3.1 Evaluation of first-order sensitivities from GEOS-Chem-hyd

The implementation of GEOS-Chem-hyd was first evaluated by comparing the first-order semi-normalized sensitivities. Emissions of select species were perturbed domain-wide in hyperdual or real space for a 24-hour model run, and the influences on surface level concentrations of select species were assessed. The sensitivities from the hyperdual approach were compared with those from the central finite difference (FD) method, which were calculated with 5% multiplicative perturbations. The first-order hyperdual sensitivities have robust agreement with the FD sensitivities when the relationship of the emissions to the concentration is expected to be linear such as for $S_{SO_2}^{SO_2}$, $S_{NO_x}^{NO_2}$, S_{ISOP}^{ISOP}, and $S_{ISOP}^{OA_{bio}}$ (Figure 2, Table 1) as evidenced by the slopes and R^2 values of the linear regression of the two sets of sensitivities approaching unity. The deviation from unity for some relationships expected to exhibit nonlinear behaviour (e.g., secondary aerosol formation) may be attributed to the model state changing with the FD method in a manner not required in the hyperdual approach. These results promise robust implementation in the dual components, so the second-order sensitivities were next evaluated to assess whether the nonlinear behaviour is captured in the second-order sensitivities themselves. This degree of agreement is consistent with the evaluations conducted by Liu et al. (2024) for CMAQ-hyd.

https://doi.org/10.5194/egusphere-2025-4543
Preprint. Discussion started: 30 October 2025

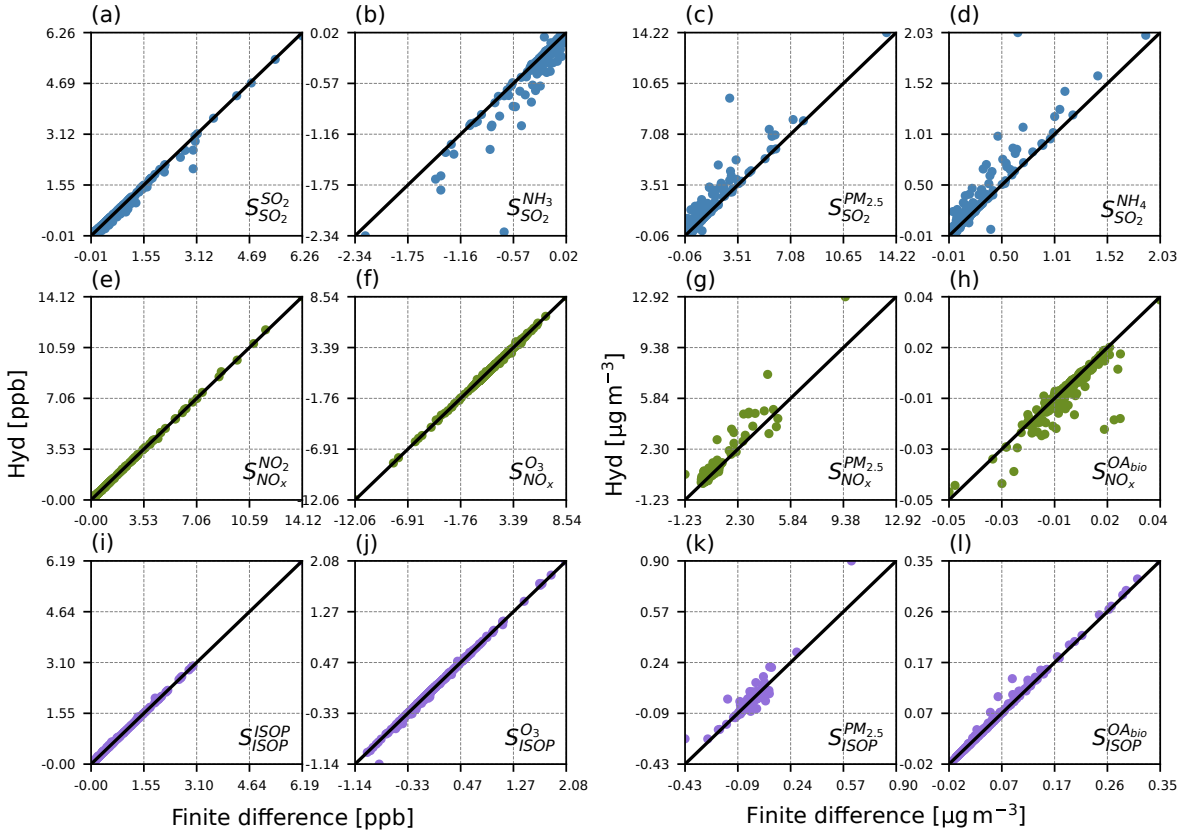

Figure 2. Comparisons of first-order semi-normalized sensitivities of the time-averaged concentration at the ground layer to the emissions throughout the 24-hour episode using the hyperdual step method (Hyd) and the central finite difference method with a 5% perturbation in each direction. The sensitivity plots are polychromed by the domain-wide perturbed emissions of SO_2, NO_x, or isoprene (ISOP) as indicated in the subscript. The superscript indicates the concentration. $\boldsymbol{OA_{bio}}$ denotes organic aerosol attributable to biogenic sources. The calculated sensitivities are labelled at the bottom right corner of each panel. The left two panels show examples of gas-phase species concentrations with respect to corresponding emissions, while the right two panels show examples of aerosol-phase products with respect to their gaseous precursors.

Table 1. The slopes and R^2 values from the linear regression of the data in each subplot of Figure 2 in the corresponding order.

First-order sensitivity: slope, R^2			
$S_{SO_2}^{SO_2}$: 0.96, 1.00	$S_{SO_2}^{NH_3}$: 1.17, 0.92	$S_{SO_2}^{PM_{2.5}}$: 1.14, 0.93	$S_{SO_2}^{NH_4}$: 1.17, 0.92
$S_{NO_x}^{NO_2}$: 1.00, 1.00	$S_{NO_x}^{O_3}$: 1.00, 1.00	$S_{NO_x}^{PM_{2.5}}$: 1.22, 0.92	$S_{NO_x}^{OA_{bio}}$: 0.95, 0.80
S_{ISOP}^{ISOP}: 1.00, 1.00	$S_{ISOP}^{O_3}$: 1.01, 1.00	$S_{ISOP}^{PM_{2.5}}$: 1.01, 1.00	$S_{ISOP}^{OA_{bio}}$: 1.02, 1.00

The HEMCO model as well as some modules within GEOS-Chem were tested and refined incrementally to obtain these results. As noted in Section 2.2, only the necessary subroutines in HEMCO were hyperdualized to propagate sensitivities from concentration-based input to emissions. The first-order sensitivities from the GEOS-Chem external arrays to the HEMCO arrays evaluate well against finite difference (Fig. S1). The aerosol thermodynamics equilibrium module, ISORROPIA, contributed to unrealistic sensitivities. These excursions were limited by maintaining the calculations in real space only within the activity coefficient calculations. By testing ISORROPIA in a standalone manner, this adjustment was shown not to alter the first- or second-

https://doi.org/10.5194/egusphere-2025-4543
Preprint. Discussion started: 30 October 2025

order sensitivities substantially in the usual case of a stable result while eliminating the rare cases in which activity coefficient calculations led to extremely large sensitivities. This approach also improved computational efficiency marginally. Similarly, the gas-phase rate constants in the kinetic preprocessor were maintained as real rather than hyperdual to the same effect.

To illustrate the impact of the model state changing in the FD approach, the spatial difference in sensitivities between the FD and hyd of ground-level, time-averaged O_3 concentrations to the domain-wide emissions of NO_x are shown with different FD perturbation sizes (Figure 3b-c). The results demonstrate clear consistency between the hyd and FD sensitivities at small perturbation sizes (105%, 95%) as shown in Fig. 3b. However, as the perturbation size increases substantially (200%, 0%), the FD sensitivities increasingly deviate from the hyd benchmark, especially in chemically nonlinear regions such as East China (Fig. 3c). This divergence highlights the compounded effects of truncation errors and significant shifts in chemical regimes caused by large perturbations. Consequently, choosing an optimal perturbation size for FD calculations requires case-by-case adjustments tailored to specific species and chemical environments. On the contrary, the hyperdual method delivers accurate sensitivities without altering the model state. Because the coarse spatial resolution and linear averaging can dampen apparent nonlinearities in gas-phase chemistry and mixing, spatial differences (Fig. 3b-c) were used to clearly highlight sensitivity variations resulting from different perturbation sizes.

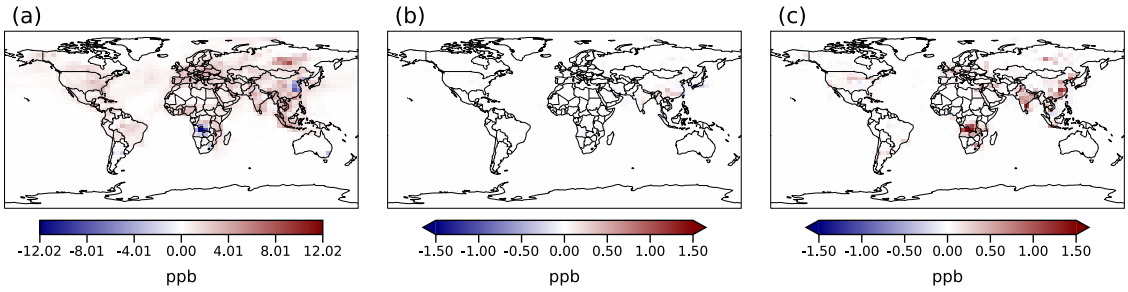

Figure 3. Map of (a) the first-order semi-normalized sensitivities of time-averaged, ground layer ozone concentrations with respect to domain-wide, persistent hyperdual perturbation of NO_x emissions. Spatial difference between the central finite difference (FD) and the hyperdual (hyd) for (b) FD sensitivities calculated with a 5% perturbation in each direction (105%, 95 %) and (c) FD sensitivities calculated with a 100 % perturbation in each direction (200 %, 0%).

Furthermore, studies commonly employ forward or backward finite difference methods (Hammer et al., 2021; Cook et al., 2020), such as the "zero out" approach, rather than the more accurate central FD method. Comparisons of these FD variants against the hyperdual sensitivities (Figure 4) reveal pronounced discrepancies, particularly for the forward and backward FD, which underscores the challenges posed by nonlinear chemical interactions. Large perturbations amplify the inaccuracies arising from these simpler finite difference methods. Additionally, the discrepancies near zero show that subtractive cancellation errors are evident (Figure 4, inset). Near zero, some data points computed using forward and backward finite differences scatter on either side of the unity line, showing that each scheme can over- or under-predict the hyperdual results depending on the local non-linearity

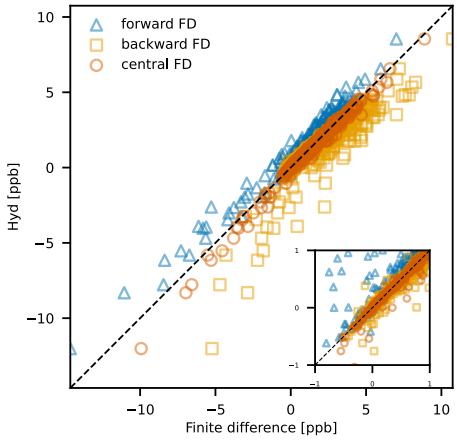

Figure 4. Comparison of first-order semi-normalized sensitivities of the time-averaged concentration at the ground layer to the emissions throughout the 24-hour episode using the hyperdual step method (Hyd) and various FD methods with a 100% perturbation in each direction.

https://doi.org/10.5194/egusphere-2025-4543
Preprint. Discussion started: 30 October 2025

and subtractive-cancellation errors. These results emphasize the advantage of the inherent precision provided by the hyperdual method.

3.2 Evaluation of second-order sensitivities from GEOS-Chem-hyd

Evaluation of the second-order and cross sensitivities from GEOS-Chem-hyd was the final step in the implementation process. The second-order sensitivities derived from GEOS-Chem-hyd were compared with the hybrid approach described in Sect. 2.3. Second-order sensitivities were effectively validated through comparisons between GEOS-Chem-hyd and the hybrid methods using one-to-one plots (Fig. 5) as was done for CMAQ-hyd (Liu et al., 2024). The hybrid method reduces the sensitivity of the second-order sensitivities to perturbation sizes (Berman et al., 2023).

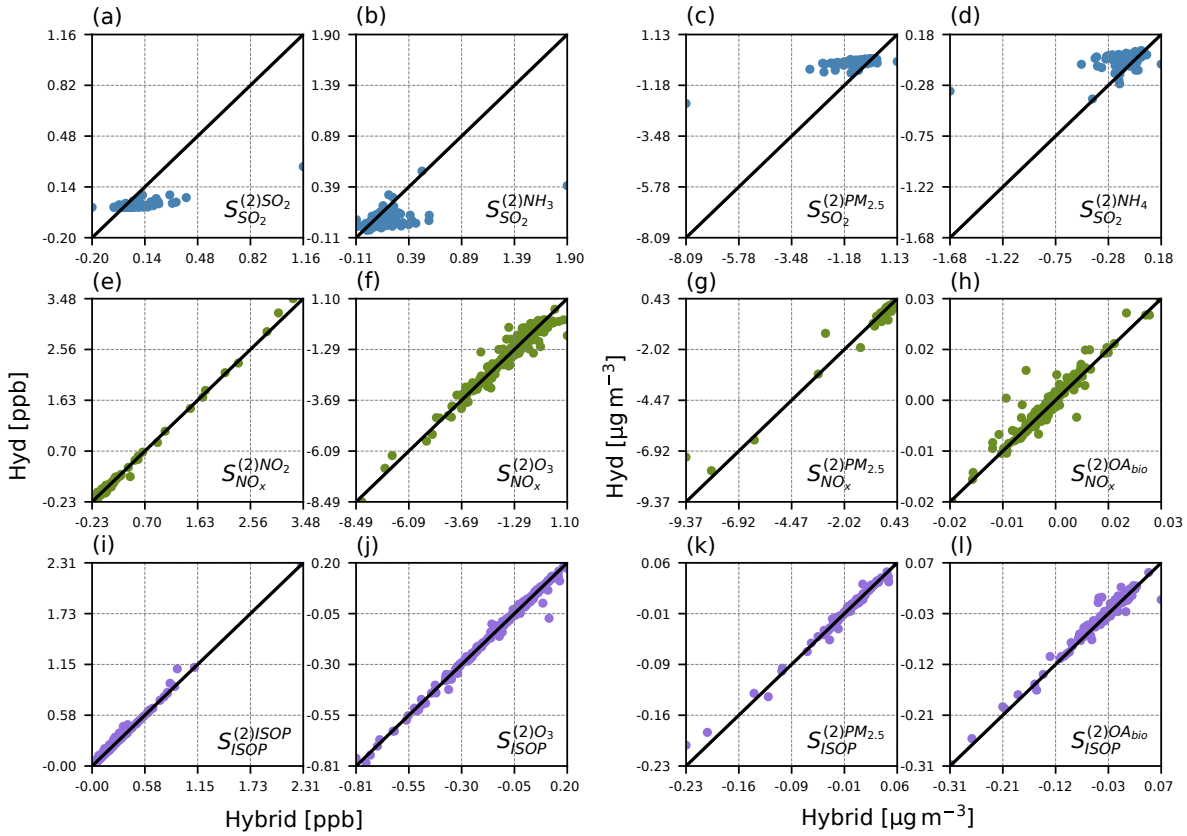

Figure 5. Comparisons of second-order semi-normalised sensitivities of the species indicated in the superscript at the ground layer averaged over the 24-hour episode to emissions of the species indicated in the subscript using the hyperdual step (Hyd) and the hybrid methods. The sensitivity plots are polychromed by the domain-wide perturbed emissions of SO_2, NO_x, or ISOP as indicated in the subscript. The calculated sensitivities are labelled in the bottom right corner of each panel. The left two panels show examples of gas-phase species concentrations with respect to corresponding emissions, while the right two panels show examples of aerosol-phase products with respect to their gaseous precursors.

https://doi.org/10.5194/egusphere-2025-4543
Preprint. Discussion started: 30 October 2025

Table 2. The slopes and R^2 values from the linear regression of the data in each subplot in Figure 4 in the corresponding order.

Second-order sensitivity: slope, R^2			
$S_{SO_2}^{(2)SO_2}$: 0.18, 0.79	$S_{SO_2}^{(2)NH_4}$: 0.26, 0.47	$S_{SO_2}^{(2)PM_{2.5}}$: 0.20, 0.78	$S_{SO_2}^{(2)NH_4}$: 0.25, 0.45
$S_{NO_x}^{(2)NO_2}$: 1.02, 1.00	$S_{NO_x}^{(2)O_3}$: 0.98, 0.97	$S_{NO_x}^{(2)PM_{2.5}}$: 0.88, 0.96	$S_{NO_x}^{(2)OA_{\mathrm{bio}}}$: 1.00, 0.91
$S_{ISOP}^{(2)ISOP}$: 1.03, 1.00	$S_{ISOP}^{(2)O_3}$: 1.00, 0.99	$S_{ISOP}^{(2)PM_{2.5}}$: 0.94, 0.99	$S_{ISOP}^{(2)OA_{bio}}$: 1.00, 0.99

The statistics of the linear regression of the data in each subplot of Figure 4 (Table 2) indicate that the agreement between hyperdual and hybrid sensitivities with respect to SO_2 are poor while those with respect to NO_x and ISOP are strong. As noted in Liu et al. (2024), the disagreement between the hybrid and hyperdual sensitivities for SO_2 is attributable to the dependence on FD within the hybrid method, which introduce disagreement in the first-order sensitivities with respect to SO_2 emissions (Fig. 2a-d). Consistent with this reasoning, the disagreement tends to reflect more spread in the hybrid results and less in the hyperdual for the second-order sensitivity relationships with respect to SO_2 emissions (Fig. 5a-d).

The agreement of the hyperdual and hybrid sensitivities is much stronger for second-order sensitivities with respect to NO_x and ISOP. The self-sensitivities, $S_{NO_x}^{(2)NO_2}$ and $S_{ISOP}^{(2)ISOP}$, show strong agreement, with slopes of 1.02 to 1.03, respectively, and both R^2 values being 1.00 (Table 2). Other gas-phase concentrations also show good agreement, consistent with nearly linear processes. The degree of agreement for $S_{NO_x}^{(2)PM_{2.5}}$ is slightly less than that for $S_{NO_x}^{(2)NO_2}$ and $S_{NO_x}^{(2)O_3}$, indicating more nonlinearity in the formation process from NO_x emissions to $PM_{2.5}$ concentrations. The $S_{NO_x}^{(2)OA_{bio}}$ relationship has a slope of 1.00 and an R^2 value of 0.91, indicating no proportional bias between the hyperdual and hybrid sensitivities but some scatter. To further investigate the impacts of model state changes and the inaccuracy inherent in the FD method, consistent with the first-order sensitivity comparisons presented in Sect 3.1, we analyzed the spatial distribution of ground layer O_3 concentrations to domain-wide perturbations of NO_x emissions (Fig. 6). Panels (b-d) illustrate the spatial differences between central second-order sensitivities derived using the central FD method and the hyd approach. Subtractive cancellation errors significantly degrade sensitivity estimates for smaller perturbation sizes (105 %, 95 %), resulting in noisy and unreliable outcomes (Fig. 6b). Although larger perturbation sizes (150 %, 95 %; 200 %, 0 %) mitigate subtractive cancellation errors to some extent, noticeable truncation errors and unintended shifts in the model state persist (Fig. 6c-d). Consequently, the second-order central FD method becomes inaccurate and unsuitable for calculating derivatives within strongly nonlinear chemical systems. In contrast, the hyperdual method provides accurate second-order sensitivities without the susceptibility to subtractive cancellation or truncation errors, preserving the original model state throughout the calculation. This comparison demonstrates the value of the independence of the hyperdual sensitivity from perturbation-induced changes to the model state.

https://doi.org/10.5194/egusphere-2025-4543
Preprint. Discussion started: 30 October 2025

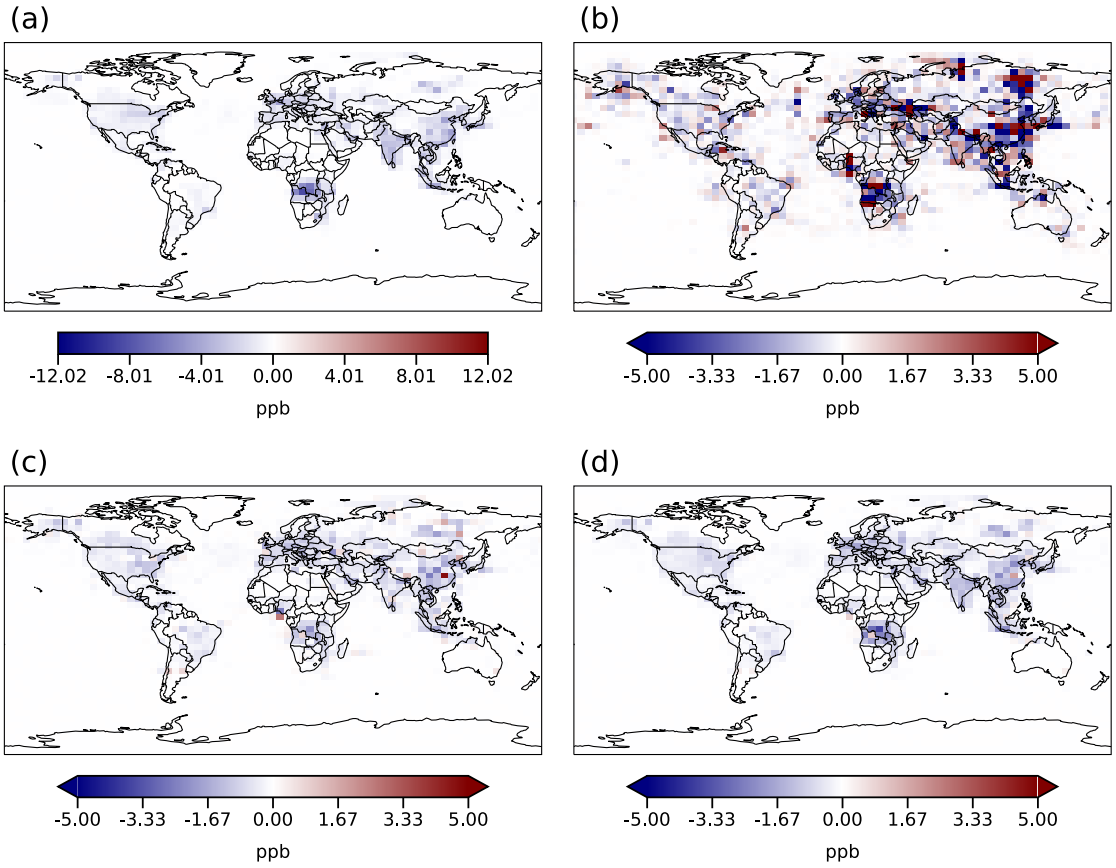

Figure 6. Map of the second-order semi-normalized sensitivities of ground layer ozone concentration averaged over the 24-hour episode with respect to domain-wide hyperdual perturbation of NO_x emissions (a). Spatial difference between the central finite difference (FD) and the hyperdual (hyd) for (b) FD sensitivities calculated with a 5% perturbation in each direction (105%, 95%), (c) FD sensitivities calculated with a 50% perturbation in each direction (150%, 50%) and (d) FD sensitivities calculated with a 100 % perturbation in each direction (200%, 0%).

3.3 Computational cost of GEOS-Chem-hyd

We assessed the overhead of the augmented GEOS-Chem-hyd model through direct comparison with the standard "base" GEOS-Chem on the National Science Foundation-supported Derecho cluster using 128 CPU cores. Both models were compiled in optimized "release" mode and executed for a 24 h simulation. Wall-time for the entire model and each major process were determined via the built-in GEOS-Chem timers (Fig. 7). Hyperdual function calculations require 4-14 times that of a real function calculation (Fike and Alonso, 2011), which depends on the complexity of the function, the compiler behaviour, and the degree of optimization.

The total wall time for GEOS-Chem-hyd was approximately 3.9 times the cost of the base GEOS-Chem run. The FD approach would require three model runs without any tuning of the perturbation size, so this computational cost is competitive. The average memory usage for the base run was 10.6 GB while that for GEOS-Chem-hyd was 32.7 GB. Selective implementation of the hyperdual type provided some efficiency gains over the expected computational and memory increases. The hyperdualized gas phase chemistry and photolysis processes increase the computational cost over the base model the most (Fig. 6). These processes include several nested loops, which may induce poor load balancing and extended computational tasks assigned to a

https://doi.org/10.5194/egusphere-2025-4543
Preprint. Discussion started: 30 October 2025

single core. The HEMCO model, which is not yet fully hyperdualized, only required 1.4 times the computational cost of the base HEMCO. Other processes had a computational requirement that would be comparable in cost to running the FD method, with the computational cost ranging from 2.3 to 4.2 times the base GEOS-Chem run.

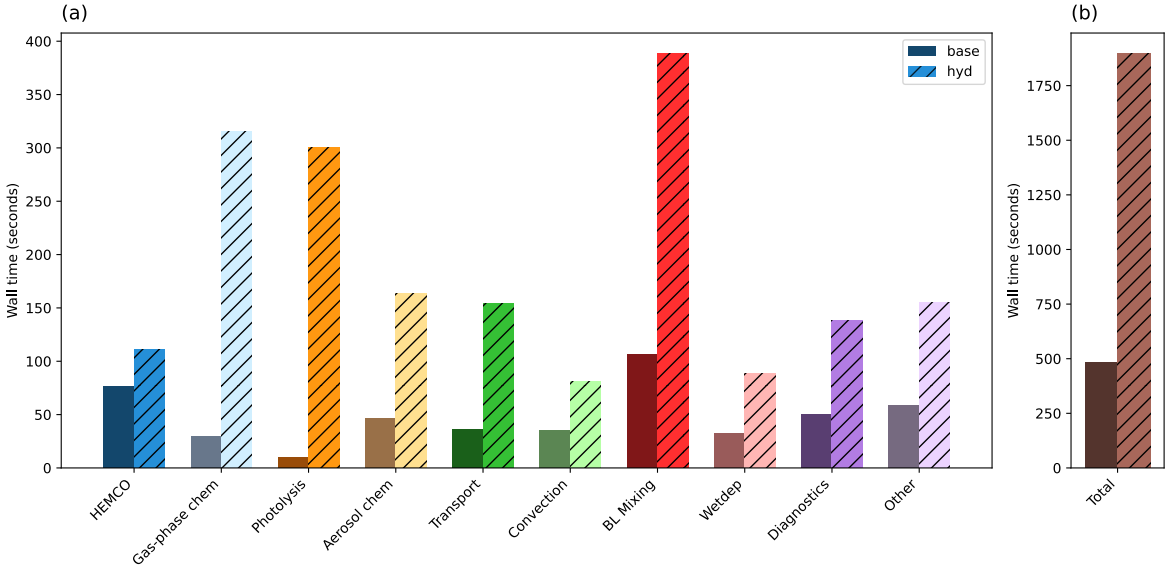

Figure 7. The computational time required for the base GEOS-Chem (left bar) in comparison to GEOS-Chem-hyd (right bar) in release mode. The wall time over a 24-hour time-averaged simulation is shown on the *y*-axis, and relevant processes are shown on the *x*-axis. The wall time for each process is shown in (a) while the total wall time for the simulations are shown in (b).

3.4 Application of GEOS-Chem-hyd

The hyperdual method efficiently provides source-oriented first-, second-, or cross sensitivities, which are complementary to the receptor-oriented sensitivities calculated with a model adjoint (Henze et al., 2007). Specifically, the hyperdual method is practical for simultaneously quantifying the impact of select input parameters on all model outputs. As such, the hyperdual method complements the adjoint by easily exploring the influence of a specific source on the entire set of concentrations (Jacobian rows), while the adjoint computes the influence on a select set of concentrations of all sources (Jacobian columns). The hyperdual approach also provides higher-order sensitivities, which would require differentiating the adjoint model or conducting numerous adjoint simulations. In contrast, the hyperdual method yields first- and second-order derivatives in a single model run, which enables the quantification of the influence of emissions of selected species on concentrations through nonlinear chemical reactions.

As an example, the influence of NO_x on key concentrations was quantified with a single GEOS-Chem-hyd simulation of August 1-8, 2019. The first- and second-order semi-normalized sensitivities of ground-layer O_3, $PM_{2.5}$, ammonium (NH_4), and biogenic organic aerosol (OA_{bio}) concentrations to NO_x emissions provide adequate information for assessing how a fractional change in domain-wide emissions would impact the concentrations in any ground layer grid cell (Figure 8).

https://doi.org/10.5194/egusphere-2025-4543
Preprint. Discussion started: 30 October 2025

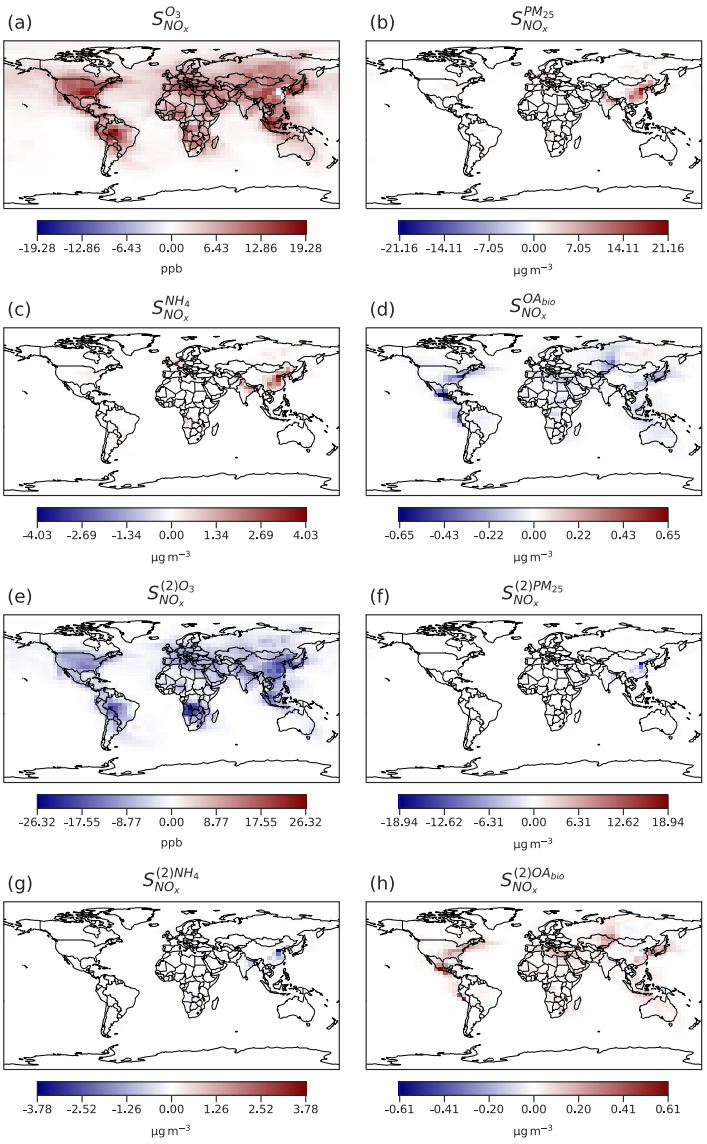

Figure 8. First- and second-order semi-normalised sensitivities of time-averaged O_3, $PM_{2.5}$, NH_4, and biogenic organic aerosol (OA_{bio}) concentrations with respect to NO_x emissions on the ground layer for a 1-week simulation. Panels (a-d) show the first-order sensitivities and (e-h) show the second-order sensitivities.

The first-order sensitivities of O_3 concentrations to NO_x emissions are predominantly positive across most regions (Fig. 8a), indicating that an increase in NO_x emissions will lead to an increase in O_3 concentration, and a reduction in NO_x emissions will lead to a reduction in O_3 concentration. However, over industrial regions in East China (Fig. 8a), the first-order sensitivities approach zero or become slightly negative due to NO_x titration effects, wherein direct emissions of NO (e.g., urban traffic or nighttime combustion) react with O_3 to temporarily decrease local O_3 concentrations. Therefore, reducing NO_x emissions in such regions does not necessarily result in lower O_3 concentrations and may inadvertently lead to an increase in O_3 concentrations due to reduced titration. The second-order sensitivities, $S_{NO_x}^{(2)O_3}$, are predominantly negative, indicating a convex nonlinear relationship. Accordingly, first-order estimates alone would indicate a larger influence of NO_x emission reductions on O_3 concentrations than would occur. For example, in the central-west region of Brazil where the first-order sensitivity is approximately 15 ppb, a 20% reduction in NO_x emissions should lead to a reduction of O_3 concentrations by 3 ppb. However, including the second-order sensitivity of around -20 ppb adjusts this estimate for a 20% reduction in NO_x emissions to a more realistic O_3 concentration reduction of approximately 2.6 ppb. For highly nonlinear processes, approximating the influence of emissions controls requires considering these higher-order terms.

The first-order sensitivity of $PM_{2.5}$ to NO_x emissions, $S_{NO_x}^{PM_{2.5}}$, is also predominantly positive (Fig. 8b). Over eastern China, the $S_{NO_x}^{PM_{2.5}}$ is largely positive, which indicates that an increase in NO_x emissions will lead to an increase in $PM_{2.5}$ concentrations. However, for the second-order sensitivities, the $S_{NO_x}^{(2)PM_{2.5}}$ (Fig. 8f) is predominantly negative, again implying potential overestimation of the contribution of NO_x emissions to $PM_{2.5}$ concentrations if neglecting the second-order term. The $S_{NO_x}^{PM_{2.5}}$ (Fig. 8b) and $S_{NO_x}^{NH_4}$ (Fig. 8c) have similar spatial patterns but a much smaller magnitude for the latter. $S_{NO_x}^{NH_4}$ indicates the extent to which

https://doi.org/10.5194/egusphere-2025-4543
Preprint. Discussion started: 30 October 2025

NOx leads to additional ammonium in the aerosol, which is only a portion of the total $PM_{2.5}$ (Li et al., 2021). Similar to $S_{NO_x}^{(2)PM_{2.5}}$ (Fig. 8f), $S_{NO_x}^{(2)NH_4}$ (Fig. 8g) are predominantly negative, which means a linear approach would overestimate the contribution of NO_x emissions to NH_4 concentrations.

The sensitivities of OA_{bio} to NO_x emissions exhibit significant regional variability. Biogenic organic aerosols are secondary organic aerosols (SOA) formed from isoprene and terpene oxidation and respond to NO_x differently depending on the region. Over the continental US, Mexico, central Africa, Europe, China, and western Asia, the $S_{NO_x}^{OA_{bio}}$ (Fig. 8d) is primarily negative, which indicates that increasing NO_x would suppress OA_{bio} formation whereas in the boreal eastern Russia, the $S_{NO_x}^{OA_{bio}}$ is somewhat positive. This contrast arises from differences in volatile organic compound precursors, oxidant chemistry, meteorology, and land cover. Boreal conifer forests emit mainly monoterpenes (e.g., α-pinene), which are oxidized by nitrate radicals (NO_3) and OH to produce low-volatility organonitrates. Laboratory and field studies show that NO_3 reacting with monoterpenes yields significant aerosol nitrates (23–44%) (Ayres et al., 2015). Thus, in regions like eastern Siberia with abundant monoterpenes and seasonally strong NO_3, adding NO_x boosts OA_{bio} via organonitrates. By contrast, in high-NO_x, isoprene-rich regions (e.g., SE US during daytime, urban plumes), NO_x often suppresses OA_{bio}. High NO_x shifts isoprene oxidation away from low-NO pathways toward volatile nitrates. Studies have shown a net effect of a lower total OA_{bio} when NO_x is high (Zhang et al., 2017; De Sá et al., 2017). In summary, NO_x enhances OA_{bio} formation where organonitrate pathways dominate (typically cooler, NO_x-limited/monoterpene areas), but can inhibit SOA where high-NO_x truncates IEPOX or OH-driven yields (warmer, VOC-rich areas). These dynamics are evident in the sensitivities from this simulation. The inhibition caused by high-NO_x can be seen in more industrial regions in the Eastern US, where there is a larger negative $S_{NO_x}^{OA_{bio}}$ compared to other regions in the country (Fig. 8d). The second-order sensitivities tend to oppose the signal of the first-order sensitivity. Generally, in regions with positive $S_{NO_x}^{(2)OA_{bio}}$ (Fig. 8h), the $S_{NO_x}^{OA_{bio}}$ is negative and vice versa. In select places like eastern China and central Peru, the negative $S_{NO_x}^{(2)OA_{bio}}$ (Fig. 8h) is much greater in magnitude than the positive $S_{NO_x}^{OA_{bio}}$ (Fig. 8d), which indicates significant nonlinearity.

By combining these sensitivities with a selected fractional, domain-wide emissions change in NOx, a Taylor series expansion would show the expected change in average concentrations of any of the species under consideration (Wang et al., 2022). The addition of accurate second-order sensitivities can help researchers and environmental decision makers develop more accurate emission control strategies for pollutants such as O_3 and $PM_{2.5}$ that respond nonlinearly to precursor emissions.

4 Conclusion

We implemented the hyperdual step method in GEOS-Chem to create GEOS-Chem-hyd. This novel approach allows for the computation of numerically exact first- and second-order sensitivities in a single model execution. GEOS-Chem-hyd provides a robust alternative to existing numerical methods, overcoming limitations such as subtractive cancellation and truncation errors inherent in the finite difference method. Moreover, it complements adjoint-based methods by efficiently addressing source-oriented sensitivities and nonlinear interactions.

The evaluations conducted demonstrated robust agreement between GEOS-Chem-hyd and established methods. First-order sensitivity comparisons with the central finite difference method showed strong alignment, particularly for linear relationships. Second-order sensitivities of nonlinear processes are difficult to evaluate so a hybrid hyperdual-central finite difference method (Berman et al., 2023) was employed. GEOS-Chem-hyd tended to show smaller spread where finite difference methods demonstrated dependence on the size of the real perturbation and subsequent model state.

https://doi.org/10.5194/egusphere-2025-4543
Preprint. Discussion started: 30 October 2025

GEOS-Chem-hyd was applied to understand the influence of domain-wide NO_x emissions on the concentrations in each ground-level grid cell of O_3, $PM_{2.5}$, NH_4, and OA_{bio}. The second-order sensitivities typically moderate the change expected from the first-order sensitivity alone. For the OA_{bio}, the sensitivities varied regionally. For example, the NO_x-induced formation of biogenic organic aerosols showed contrasting regional responses dependent on precursor chemistry, oxidant availability, and meteorological conditions. In short, this application demonstrates that GEOS-Chem-hyd may provide insights for environmental decisionmaker seeking to optimize emission reduction strategies or scientists estimating the influence of an emission on a pollutant of interest.

The computational cost of GEOS-Chem-hyd is approximately four times that of the base model. Strategic variable conversion limited the overhead associated with hyperdual calculations. Accordingly, GEOS-Chem-hyd is competitive with existing sensitivity analysis methods. Future work includes fully integrating the hyperdual method within the Harmonized Emissions Component (HEMCO) for sector-specific applications.

Overall, GEOS-Chem-hyd represents a substantial advancement for atmospheric sensitivity analysis in a widely used global CTM, offering precise insights into pollutant dynamics in a computationally feasible manner. GEOS-Chem developers may also find this augmented version useful for debugging the implementation of new code or for assessing the impact of a scientific advancement newly implemented in the model. Its accurate second-order sensitivities are valuable for understanding complex atmospheric chemistry interactions and improving the effectiveness of policy interventions aimed at mitigating air pollution impacts.

Code and Data Availability. GEOS-Chem version 14.0.0 is available at https://github.com/geoschem/geos-chem/releases/tag/14.0.0, and is archived at https://doi.org/10.5281/zenodo.7254984. GEOS-Chem-hyd is archived at https://doi.org/10.5281/zenodo.16575028 (Akinjole and Capps, 2025). Both the GEOS-Chem and the GEOS-Chem-hyd models are under MIT licenses. The input data configuration for the simulation experiments is available at https://doi.org/10.5281/zenodo.16575028 (Akinjole and Capps, 2025).

Author contribution. SOA developed the model code, performed the simulations, and developed the figures with direction from SLC. SOA initially drafted the manuscript which SLC significantly revised.

Competing Interests. The authors declare that they have no conflict of interest.

Acknowledgements. The work is supported by National Science Foundation CAREER Award Grant No. 1944669. The authors would also like to thank Dr. Ryan P. Russell for kindly providing the testing framework of multicomplex numbers, which inspired the development of the testing framework for hyperdual numbers, and Dr. Sebastian D. Eastham, who created the standalone framework that was used for testing ISORROPIA-hyd.

https://doi.org/10.5194/egusphere-2025-4543
Preprint. Discussion started: 30 October 2025

References

Akinjole, S. O. and Capps, S. L.: GEOS-Chem-14.0.0-hyd (1.0.0), Zenodo [code], https://doi.org/10.5281/zenodo.16575028, 2025.

Alexe, M. and Sandu, A.: On the discrete adjoints of adaptive time stepping algorithms, J. Comput. Appl. Math., 233, 1005-1020, 10.1016/j.cam.2009.08.109, 2009.

Anenberg, S. C., Miller, J., Henze, D. K., Minjares, R., and Achakulwisut, P.: The global burden of transportation tailpipe emissions on air pollution-related mortality in 2010 and 2015, Environmental Research Letters, 14, 12, 10.1088/1748-9326/ab35fc, 2019.

Ayres, B. R., Allen, H. M., Draper, D. C., Brown, S. S., Wild, R. J., Jimenez, J. L., Day, D. A., Campuzano-Jost, P., Hu, W., De Gouw, J., Koss, A., Cohen, R. C., Duffey, K. C., Romer, P., Baumann, K., Edgerton, E., Takahama, S., Thornton, J. A., Lee, B. H., Lopez-Hilfiker, F. D., Mohr, C., Wennberg, P. O., Nguyen, T. B., Teng, A., Goldstein, A. H., Olson, K., and Fry, J. L.: Organic nitrate aerosol formation via NO_3 + biogenic volatile organic compounds in the southeastern United States, Atmospheric Chemistry and Physics, 15, 13377-13392, 10.5194/acp-15-13377-2015, 2015.

Berman, B., Capps, S. L., Sauvageau, I., Gao, E., Eastham, S. D., and Russell, R. P.: ISORROPIA-MCX: Enabling Sensitivity Analysis With Multicomplex Variables in the Aerosol Thermodynamic Model, ISORROPIA, Earth and Space Science, 10, e2022EA002729, https://doi.org/10.1029/2022EA002729, 2023.

Bey, I., Jacob, D. J., Yantosca, R. M., Logan, J. A., Field, B. D., Fiore, A. M., Li, Q. B., Liu, H. G. Y., Mickley, L. J., and Schultz, M. G.: Global modeling of tropospheric chemistry with assimilated meteorology: Model description and evaluation, Journal of Geophysical Research-Atmospheres, 106, 23073-23095, 10.1029/2001jd000807, 2001.

Bousserez, N. and Henze, D. K.: Optimal and scalable methods to approximate the solutions of large-scale Bayesian problems: theory and application to atmospheric inversion and data assimilation, Quarterly Journal of the Royal Meteorological Society, 144, 365-390, 10.1002/qj.3209, 2018.

Brauer, M., Amann, M., Burnett, R. T., Cohen, A., Dentener, F., Ezzati, M., Henderson, S. B., Krzyzanowski, M., Martin, R. V., Van Dingenen, R., Van Donkelaar, A., and Thurston, G. D.: Exposure Assessment for Estimation of the Global Burden of Disease Attributable to Outdoor Air Pollution, Environmental Science & Technology, 46, 652-660, 10.1021/es2025752, 2012.

Burnett, R. T., Pope, C. A., Ezzati, M., Olives, C., Lim, S. S., Mehta, S., Shin, H. H., Singh, G., Hubbell, B., Brauer, M., Anderson, H. R., Smith, K. R., Balmes, J. R., Bruce, N. G., Kan, H., Laden, F., Prüss-Ustün, A., Turner, M. C., Gapstur, S. M., Diver, W. R., and Cohen, A.: An Integrated Risk Function for Estimating the Global Burden of Disease Attributable to Ambient Fine Particulate Matter Exposure, Environmental Health Perspectives, 122, 397-403, doi:10.1289/ehp.1307049, 2014.

Capps, S. L., Hu, Y., and Russell, A. G.: Assessing Near-Field and Downwind Impacts of Reactivity-Based Substitutions, Journal of the Air & Waste Management Association, 60, 316-327, 10.3155/1047-3289.60.3.316, 2010.

Carter, T. S., Heald, C. L., Cappa, C. D., Kroll, J. H., Campos, T. L., Coe, H., Cotterell, M., Davies, N. W., Farmer, D. K., Fox, C., Garofalo, L. A., Hu, L., Langridge, J. M., Levin, E. J. T., Murphy, S. M., Pokhrel, R. P., Shen, Y. J., Szpek, K., Taylor, J. W., and Wu, H. H.: Investigating Carbonaceous Aerosol and Its Absorption Properties From Fires in the Western United States (WE-CAN) and Southern Africa (ORACLES and CLARIFY), Journal of Geophysical Research-Atmospheres, 126, 10.1029/2021jd034984, 2021.

Chen, Y., Shen, H., Kaiser, J., Hu, Y., Capps, S. L., Zhao, S., Hakami, A., Shih, J.-S., Pavur, G. K., Turner, M. D., Henze, D. K., Resler, J., Nenes, A., Napelenok, S. L., Bash, J. O., Fahey, K. M., Carmichael, G. R., Chai, T., Clarisse, L., Coheur, P.-F., Van Damme, M., and Russell, A. G.: High-resolution hybrid inversion of IASI ammonia columns to constrain US ammonia emissions using the CMAQ adjoint model, Atmospheric Chemistry and Physics, 21, 2067-2082, 10.5194/acp-21-2067-2021, 2021.

Cheng, Y., Wang, Y. H., Zhang, Y. Z., Crawford, J. H., Diskin, G. S., Weinheimer, A. J., and Fried, A.: Estimator of Surface Ozone Using Formaldehyde and Carbon Monoxide Concentrations Over the Eastern United States in Summer, Journal of Geophysical Research-Atmospheres, 123, 7642-7655, 10.1029/2018jd028452, 2018.

Choi, J., Henze, D. K., Cao, H. S., Nowlan, C. R., Abad, G. G., Kwon, H. A., Lee, H. M., Oak, Y. J., Park, R. J., Bates, K. H., Maasakkers, J. D., Wisthaler, A., and Weinheimer, A. J.: An Inversion Framework for Optimizing Non-Methane VOC Emissions Using Remote Sensing and Airborne Observations in Northeast Asia During the KORUS-AQ Field Campaign, Journal of Geophysical Research-Atmospheres, 127, 27, 10.1029/2021jd035844, 2022.

Constantin, B. V. and Barrett, S. R. H.: Application of the complex step method to chemistry-transport modeling, Atmospheric Environment, 99, 457-465, 10.1016/j.atmosenv.2014.10.017, 2014.

Cook, R., Phillips, S., Strum, M., Eyth, A., and Thurman, J.: Contribution of mobile sources to secondary formation of carbonyl compounds, Journal of the Air & Waste Management Association, 70, 1356-1366, 10.1080/10962247.2020.1813839, 2020.

Cooper, M., Martin, R. V., Padmanabhan, A., and Henze, D. K.: Comparing mass balance and adjoint methods for inverse modeling of nitrogen dioxide columns for global nitrogen oxide emissions, Journal of Geophysical Research: Atmospheres, 122, 4718-4734, 10.1002/2016jd025985, 2017.

Croft, B., Pierce, J. R., and Martin, R. V.: Interpreting aerosol lifetimes using the GEOS-Chem model and constraints from radionuclide measurements, Atmospheric Chemistry and Physics, 14, 4313-4325, 10.5194/acp-14-4313-2014, 2014.

De Sá, S. S., Palm, B. B., Campuzano-Jost, P., Day, D. A., Newburn, M. K., Hu, W., Isaacman-Vanwertz, G., Yee, L. D., Thalman, R., Brito, J., Carbone, S., Artaxo, P., Goldstein, A. H., Manzi, A. O., Souza, R. A. F., Mei, F., Shilling, J. E., Springston, S. R., Wang, J., Surratt, J. D., Alexander, M. L., Jimenez, J. L., and Martin, S. T.: Influence of urban pollution on the production

of organic particulate matter from isoprene epoxydiols in central Amazonia, Atmospheric Chemistry and Physics, 17, 6611-6629, 10.5194/acp-17-6611-2017, 2017.

Ding, D., Xing, J., Wang, S. X., Liu, K. Y., and Hao, J. M.: Estimated Contributions of Emissions Controls, Meteorological Factors, Population Growth, and Changes in Baseline Mortality to Reductions in Ambient PM2.5 and PM2.5-Related Mortality in China, 2013-2017, Environmental Health Perspectives, 127, 12, 10.1289/ehp4157, 2019.

Dunker, A. M., Yarwood, G., Ortmann, J. P., and Wilson, G. M.: The Decoupled Direct Method for Sensitivity Analysis in a Three-Dimensional Air Quality Model Implementation, Accuracy, and Efficiency, Environmental Science & Technology, 36, 2965-2976, 10.1021/es0112691, 2002.

Elbern, H., Schwinger, J., and Botchorishvili, R.: Chemical state estimation for the middle atmosphere by four-dimensional variational data assimilation: System configuration, Journal of Geophysical Research, 115, 23, 10.1029/2009jd011953, 2010.

Errico, R. M.: What Is an Adjoint Model?, Bulletin of the American Meteorological Society, 78, 2577-2591, 10.1175/1520-0477(1997)078<2577:wiaam>2.0.co;2, 1997.

Field, R. D., van der Werf, G. R., Fanin, T., Fetzer, E. J., Fuller, R., Jethva, H., Levy, R., Livesey, N. J., Luo, M., Torres, O., and Worden, H. M.: Indonesian fire activity and smoke pollution in 2015 show persistent nonlinear sensitivity to El Nino-induced drought, Proc. Natl. Acad. Sci. U. S. A., 113, 9204-9209, 10.1073/pnas.1524888113, 2016.

Fike, J. A. and Alonso, J. J.: The Development of Hyper-Dual Numbers for Exact Second-Derivative Calculations, 49th AIAA Aerospace Sciences Meeting including the New Horizons Forum and Aerospace Exposition, Orlando, Florida, 4-7 January, 10.2514/6.2011-886, 2011.

Fisher, J. A., Murray, L. T., Jones, D. B. A., and Deutscher, N. M.: Improved method for linear carbon monoxide simulation and source attribution in atmospheric chemistry models illustrated using GEOS-Chem v9, Geoscientific Model Development, 10, 4129-4144, 10.5194/gmd-10-4129-2017, 2017.

Fountoukis, C. and Nenes, A.: ISORROPIA II: a computationally efficient thermodynamic equilibrium model for K^+–Ca^{2+}–Mg^{2+}–NH_4–Na^+–SO_4^{2-}–NO_3^- –Cl^-–H_2O aerosols, Atmospheric Chemistry and Physics, 7, 4639-4659, 10.5194/acp-7-4639-2007, 2007.

Fu, J. S., Carmichael, G. R., Dentener, F., Aas, W., Andersson, C., Barrie, L. A., Cole, A., Galy-Lacaux, C., Geddes, J., Itahashi, S., Kanakidou, M., Labrador, L., Paulot, F., Schwede, D., Tan, J. N., and Vet, R.: Improving Estimates of Sulfur, Nitrogen, and Ozone Total Deposition through Multi-Model and Measurement-Model Fusion Approaches, Environmental Science & Technology, 56, 2134-2142, 10.1021/acs.est.1c05929, 2022.

Gelaro, R., McCarty, W., Suárez, M. J., Todling, R., Molod, A., Takacs, L., Randles, C. A., Darmenov, A., Bosilovich, M. G., Reichle, R., Wargan, K., Coy, L., Cullather, R., Draper, C., Akella, S., Buchard, V., Conaty, A., da Silva, A. M., Gu, W., Kim, G.-K., Koster, R., Lucchesi, R., Merkova, D., Nielsen, J. E., Partyka, G., Pawson, S., Putman, W., Rienecker, M., Schubert, S. D., Sienkiewicz, M., and Zhao, B.: The Modern-Era Retrospective Analysis for Research and Applications, Version 2 (MERRA-2), Journal of Climate, 30, 5419-5454, https://doi.org/10.1175/JCLI-D-16-0758.1, 2017.

Giering, R. and Kaminski, T.: Recipes for adjoint code construction, ACM Transactions on Mathematical Software, 24, 437-474, 10.1145/293686.293695, 1998.

Giles, M. B. and Pierce, N. A.: An Introduction to the Adjoint Approach to Design, Flow, Turbulence and Combustion, 65, 393-415, 10.1023/A:1011430410075, 2000.

Hakami, A., Odman, M. T., and Russell, A. G.: Nonlinearity in atmospheric response: A direct sensitivity analysis approach, Journal of Geophysical Research: Atmospheres, 109, 10.1029/2003JD004502, 2004.

Hammer, M. S., Donkelaar, A. v., Martin, R. V., McDuffie, E. E., Lyapustin, A., Sayer, A. M., Hsu, N. C., Levy, R. C., Garay, M. J., Kalashnikova, O. V., and Kahn, R. A.: Effects of COVID-19 lockdowns on fine particulate matter concentrations, Science Advances, 7, eabg7670, doi:10.1126/sciadv.abg7670, 2021.

Han, H., Liu, J., Yuan, H. L., Wang, T. J., Zhuang, B. L., and Zhang, X.: Foreign influences on tropospheric ozone over East Asia through global atmospheric transport, Atmospheric Chemistry and Physics, 19, 12495-12514, 10.5194/acp-19-12495-2019, 2019.

Hascoët, L. and Dauvergne, B.: Adjoints of large simulation codes through Automatic Differentiation, Eur. J. Comput. Mech., 17, 63-86, 10.3166/remn.17.63-86, 2008.

Heimbach, P., Hill, C., and Giering, R.: An efficient exact adjoint of the parallel MIT General Circulation Model, generated via automatic differentiation, Futur. Gener. Comp. Syst., 21, 1356-1371, 10.1016/j.future.2004.11.010, 2005.

Henze, D. K., Hakami, A., and Seinfeld, J. H.: Development of the adjoint of GEOS-Chem, Atmos. Chem. Phys., 7, 2413-2433, 10.5194/acp-7-2413-2007, 2007.

Henze, D. K., Seinfeld, J. H., and Shindell, D. T.: Inverse modeling and mapping US air quality influences of inorganic PM2.5 precursor emissions using the adjoint of GEOS-Chem, Atmospheric Chemistry and Physics, 9, 5877-5903, 2009.

IHME: Institute for Health Metrics and Evaluation (IHME). GBD Results, 2024.

Ikeda, K., Tanimoto, H., Sugita, T., Akiyoshi, H., Kanaya, Y., Zhu, C. M., and Taketani, F.: Tagged tracer simulations of black carbon in the Arctic: transport, source contributions, and budget, Atmospheric Chemistry and Physics, 17, 10515-10533, 10.5194/acp-17-10515-2017, 2017.

Jacob, D. J., Liu, H., Mari, C., and Yantosca, R. M.: Havard wet deposition scheme for GMI, 2000.

Jaeglé, L., Shah, V., Thornton, J. A., Lopez-Hilfiker, F. D., Lee, B. H., Mcduffie, E. E., Fibiger, D., Brown, S. S., Veres, P., Sparks, T. L., Ebben, C. J., Wooldridge, P. J., Kenagy, H. S., Cohen, R. C., Weinheimer, A. J., Campos, T. L., Montzka, D. D.,

https://doi.org/10.5194/egusphere-2025-4543
Preprint. Discussion started: 30 October 2025

Digangi, J. P., Wolfe, G. M., Hanisco, T., Schroder, J. C., Campuzano-Jost, P., Day, D. A., Jimenez, J. L., Sullivan, A. P., Guo, H., and Weber, R. J.: Nitrogen Oxides Emissions, Chemistry, Deposition, and Export Over the Northeast United States During the WINTER Aircraft Campaign, Journal of Geophysical Research: Atmospheres, 123, 12,368-312,393, 10.1029/2018jd029133, 2018.

Johnson, M. S., Kuang, S., Wang, L. H., and Newchurch, M. J.: Evaluating Summer-Time Ozone Enhancement Events in the Southeast United States, Atmosphere, 7, 19, 10.3390/atmos7080108, 2016.

Keller, C. A., Evans, M. J., Knowland, K. E., Hasenkopf, C. A., Modekurty, S., Lucchesi, R. A., Oda, T., Franca, B. B., Mandarino, F. C., Suarez, M. V. D., Ryan, R. G., Fakes, L. H., and Pawson, S.: Global impact of COVID-19 restrictions on the surface concentrations of nitrogen dioxide and ozone, Atmospheric Chemistry and Physics, 21, 3555-3592, 10.5194/acp-21-3555-2021, 2021.

Kharol, S. K., Martin, R. V., Philip, S., Vogel, S., Henze, D. K., Chen, D., Wang, Y., Zhang, Q., and Heald, C. L.: Persistent sensitivity of Asian aerosol to emissions of nitrogen oxides, Geophysical Research Letters, 40, 1021-1026, 10.1002/grl.50234, 2013.

Kim, S. Y., Lee, S. D., Lee, J. B., Kim, D. R., Han, J. S., Choi, K. H., and Song, C. K.: Analysis of Long-Range Transport of Carbon Dioxide and Its High Concentration Events over East Asian Region Using GOSAT Data and GEOS-Chem Modeling, Adv. Meteorol., 2015, 13, 10.1155/2015/680264, 2015.

Koo, B., Dunker, A. M., and Yarwood, G.: Implementing the decoupled direct method for sensitivity analysis in a particulate matter air quality model, Environ Sci Technol, 41, 2847-2854, 10.1021/es0619962, 2007.

Lantoine, G., Russell, R. P., and Dargent, T.: Using Multicomplex Variables for Automatic Computation of High-Order Derivatives, ACM Transactions on Mathematical Software, 38, 1-21, 10.1145/2168773.2168774, 2012.

Lapina, K., Henze, D. K., Milford, J. B., Huang, M., Lin, M., Fiore, A. M., Carmichael, G., Pfister, G. G., and Bowman, K.: Assessment of source contributions to seasonal vegetative exposure to ozone in the U.S, Journal of Geophysical Research: Atmospheres, 119, 324-340, 10.1002/2013jd020905, 2014.

Le, T. H., Wang, Y., Liu, L., Yang, J. N., Yung, Y. L., Li, G. H., and Seinfeld, J. H.: Unexpected air pollution with marked emission reductions during the COVID-19 outbreak in China, Science, 369, 702-+, 10.1126/science.abb7431, 2020.

Li, C., Martin, R. V., Shephard, M. W., Cady-Pereira, K., Cooper, M. J., Kaiser, J., Lee, C. J., Zhang, L., and Henze, D. K.: Assessing the Iterative Finite Difference Mass Balance and 4D-Var Methods to Derive Ammonia Emissions Over North America Using Synthetic Observations, Journal of Geophysical Research-Atmospheres, 124, 4222-4236, 10.1029/2018jd030183, 2019.

Li, M., Zhang, Z., Yao, Q., Wang, T., Xie, M., Li, S., Zhuang, B., and Han, Y.: Nonlinear responses of particulate nitrate to NO_x emission controls in the megalopolises of China, Atmospheric Chemistry and Physics, 21, 15135-15152, 10.5194/acp-21-15135-2021, 2021.

Lin, H., Jacob, D. J., Lundgren, E. W., Sulprizio, M. P., Keller, C. A., Fritz, T. M., Eastham, S. D., Emmons, L. K., Campbell, P. C., Baker, B., Saylor, R. D., and Montuoro, R.: Harmonized Emissions Component (HEMCO) 3.0 as a versatile emissions component for atmospheric models: application in the GEOS-Chem, NASA GEOS, WRF-GC, CESM2, NOAA GEFS-Aerosol, and NOAA UFS models, Geoscientific Model Development, 14, 5487-5506, 10.5194/gmd-14-5487-2021, 2021.

Lin, J.-T. and McElroy, M. B.: Impacts of boundary layer mixing on pollutant vertical profiles in the lower troposphere: Implications to satellite remote sensing, Atmospheric Environment, 44, 1726-1739, https://doi.org/10.1016/j.atmosenv.2010.02.009, 2010.

Lin, S.-J. and Rood, R. B.: Multidimensional Flux-Form Semi-Lagrangian Transport Schemes, Monthly Weather Review, 124, 2046-2070, https://doi.org/10.1175/1520-0493(1996)124<2046:MFFSLT>2.0.CO;2, 1996.

Liu, H., Jacob, D. J., Bey, I., and Yantosca, R. M.: Constraints from ^{210}Pb and ^{7}Be on wet deposition and transport in a global three-dimensional chemical tracer model driven by assimilated meteorological fields, Journal of Geophysical Research: Atmospheres, 106, 12109-12128, 10.1029/2000jd900839, 2001.

Liu, J., Chen, E., and Capps, S. L.: The first application of a numerically exact, higher-order sensitivity analysis approach for atmospheric modelling: implementation of the hyperdual-step method in the Community Multiscale Air Quality Model (CMAQ) version 5.3.2, Geosci. Model Dev., 17, 567-585, 10.5194/gmd-17-567-2024, 2024.

Lyu, C., Capps, S. L., Hakami, A., Zhao, S., Resler, J., Carmichael, G. R., Sandu, A., Russell, A. G., Chai, T., and Henze, D. K.: Elucidating emissions control strategies for ozone to protect human health and public welfare within the continental United States, Environmental Research Letters, 14, 124093, 10.1088/1748-9326/ab5e05, 2019.

Lyu, C., Capps, S. L., Kurashima, K., Henze, D. K., Pierce, G., Hakami, A., Zhao, S., Resler, J., Carmichael, G. R., Sandu, A., Russell, A. G., Chai, T., and Milford, J.: Evaluating oil and gas contributions to ambient nonmethane hydrocarbon mixing ratios and ozone-related metrics in the Colorado Front Range, Atmospheric Environment, 246, 118113, https://doi.org/10.1016/j.atmosenv.2020.118113, 2021.

Mao, Y. H., Li, Q. B., Henze, D. K., Jiang, Z., Jones, D. B. A., Kopacz, M., He, C., Qi, L., Gao, M., Hao, W. M., and Liou, K. N.: Estimates of black carbon emissions in the western United States using the GEOS-Chem adjoint model, Atmospheric Chemistry and Physics, 15, 7685-7702, 10.5194/acp-15-7685-2015, 2015.

Martins, J. R. R. A., Sturdza, P., and Alonso, J. J.: The complex-step derivative approximation, ACM Trans. Math. Softw., 29, 245-262, 10.1145/838250.838251, 2003.

https://doi.org/10.5194/egusphere-2025-4543
Preprint. Discussion started: 30 October 2025

Moon, J., Choi, Y., Jeon, W., Kim, H. C., Pouyaei, A., Jung, J., Pan, S., Kim, S., Kim, C. H., Bak, J., Yoo, J. W., Park, J., and Kim, D.: Hybrid IFDMB/4D-Var inverse modeling to constrain the spatiotemporal distribution of CO and NO2 emissions using the CMAQ adjoint model, Atmospheric Environment, 327, 10, 10.1016/j.atmosenv.2024.120490, 2024.

Napelenok, S. L., Cohan, D. S., Hu, Y., and Russell, A. G.: Decoupled direct 3D sensitivity analysis for particulate matter (DDM-3D/PM), Atmospheric Environment, 40, 6112-6121, https://doi.org/10.1016/j.atmosenv.2006.05.039, 2006.

O'Rourke, P. R., Smith, S. J., Mott, A., Ahsan, H., McDuffie, E. E., Crippa, M., Klimont, Z., McDonald, B., Wang, S., Nicholson, M. B., Feng, L., and Hoesly, R. M.: CEDS v_2021_04_21 Release Emission Data (v_2021_02_05) [dataset], 10.5281/zenodo.4741285, 2021.

Pai, S. J., Heald, C. L., and Murphy, J. G.: Exploring the Global Importance of Atmospheric Ammonia Oxidation, Acs Earth and Space Chemistry, 5, 1674-1685, 10.1021/acsearthspacechem.1c00021, 2021.

Park, S.-Y., Kim, D.-H., Lee, S.-H., and Lee, H. W.: Variational data assimilation for the optimized ozone initial state and the short-time forecasting, Atmospheric Chemistry and Physics, 16, 3631-3649, 10.5194/acp-16-3631-2016, 2016.

Philip, S., Martin, R. V., and Keller, C. A.: Sensitivity of chemistry-transport model simulations to the duration of chemical and transport operators: a case study with GEOS-Chem v10-01, Geoscientific Model Development, 9, 1683-1695, 10.5194/gmd-9-1683-2016, 2016.

Pusede, S. E., Duffey, K. C., Shusterman, A. A., Saleh, A., Laughner, J. L., Wooldridge, P. J., Zhang, Q., Parworth, C. L., Kim, H., Capps, S. L., Valin, L. C., Cappa, C. D., Fried, A., Walega, J., Nowak, J. B., Weinheimer, A. J., Hoff, R. M., Berkoff, T. A., Beyersdorf, A. J., Olson, J., Crawford, J. H., and Cohen, R. C.: On the effectiveness of nitrogen oxide reductions as a control over ammonium nitrate aerosol, Atmospheric Chemistry and Physics, 16, 2575-2596, 10.5194/acp-16-2575-2016, 2016.

Pye, H. O. T., Liao, H., Wu, S., Mickley, L. J., Jacob, D. J., Henze, D. K., and Seinfeld, J. H.: Effect of changes in climate and emissions on future sulfate-nitrate-ammonium aerosol levels in the United States, Journal of Geophysical Research: Atmospheres, 114, 10.1029/2008jd010701, 2009.

Qu, Z., Henze, D. K., Capps, S. L., Wang, Y., Xu, X. G., Wang, J., and Keller, M.: Monthly top-down NOx emissions for China (2005-2012): A hybrid inversion method and trend analysis, Journal of Geophysical Research-Atmospheres, 122, 4600-4625, 10.1002/2016jd025852, 2017.

Sandu, A. and Sander, R.: Technical note: Simulating chemical systems in Fortran90 and Matlab with the Kinetic PreProcessor KPP-2.1, Atmospheric Chemistry and Physics, 6, 187-195, 10.5194/acp-6-187-2006, 2006.

Schiferl, L. D., Heald, C. L., Nowak, J. B., Holloway, J. S., Neuman, J. A., Bahreini, R., Pollack, I. B., Ryerson, T. B., Wiedinmyer, C., and Murphy, J. G.: An investigation of ammonia and inorganic particulate matter in California during the CalNex campaign, Journal of Geophysical Research-Atmospheres, 119, 1883-1902, 10.1002/2013jd020765, 2014.

Seinfeld, J. H. and Pandis, S. N., 1963-: Atmospheric chemistry and physics: from air pollution to climate change, Third edition, Hoboken, New Jersey : John Wiley & Sons2016.

Shrivastava, M., Cappa, C. D., Fan, J. W., Goldstein, A. H., Guenther, A. B., Jimenez, J. L., Kuang, C., Laskin, A., Martin, S. T., Ng, N. L., Petaja, T., Pierce, J. R., Rasch, P. J., Roldin, P., Seinfeld, J. H., Shilling, J., Smith, J. N., Thornton, J. A., Volkamer, R., Wang, J., Worsnop, D. R., Zaveri, R. A., Zelenyuk, A., and Zhang, Q.: Recent advances in understanding secondary organic aerosol: Implications for global climate forcing, Reviews of Geophysics, 55, 509-559, 10.1002/2016rg000540, 2017.

Sitwell, M., Shephard, M. W., Rochon, Y., Cady-Pereira, K., and Dammers, E.: An ensemble-variational inversion system for the estimation of ammonia emissions using CrIS satellite ammonia retrievals, Atmospheric Chemistry and Physics, 22, 6595-6624, 10.5194/acp-22-6595-2022, 2022.

Squire, W. and Trapp, G.: Using Complex Variables to Estimate Derivatives of Real Functions, SIAM Review, 40, 110-112, 10.1137/s003614459631241x, 1998.

Sun, H. W., Eastham, S., and Keith, D.: Developing a Plume-in-Grid Model for Plume Evolution in the Stratosphere, Journal of Advances in Modeling Earth Systems, 14, 17, 10.1029/2021ms002816, 2022.

Tian, D., Cohan, D. S., Napelenok, S., Bergin, M., Hu, Y. T., Chang, M., and Russell, A. G.: Uncertainty Analysis of Ozone Formation and Response to Emission Controls Using Higher-Order Sensitivities, Journal of the Air & Waste Management Association, 60, 797-804, 10.3155/1047-3289.60.7.797, 2010.

Tsimpidi, A. P., Karydis, V. A., and Pandis, S. N.: Response of inorganic fine particulate matter to emission changes of sulfur dioxide and ammonia: The eastern United States as a case study, Journal of the Air & Waste Management Association, 57, 1489-1498, 10.3155/1047-3289.57.12.1489, 2007.

Turner, M. D., Henze, D. K., Capps, S. L., Hakami, A., Zhao, S., Resler, J., Carmichael, G. R., Stanier, C. O., Baek, J., Sandu, A., Russell, A. G., Nenes, A., Pinder, R. W., Napelenok, S. L., Bash, J. O., Percell, P. B., and Chai, T.: Premature deaths attributed to source-specific BC emissions in six urban US regions, Environmental Research Letters, 10, 10.1088/1748-9326/10/11/114014, 2015.

Utke, J., Naumann, U., Fagan, M., Tallent, N., Strout, M., Heimbach, P., Hill, C., and Wunsch, C.: OpenAD/F: A modular open-source tool for automatic differentiation of Fortran codes, Acm Transactions on Mathematical Software, 34, 36, 10.1145/1377596.1377598, 2008.

van der Graaf, S., Dammers, E., Segers, A., Kranenburg, R., Schaap, M., Shephard, M. W., and Erisman, J. W.: Data assimilation of CrIS NH3 satellite observations for improving spatiotemporal NH3 distributions in LOTOS-EUROS, Atmospheric Chemistry and Physics, 22, 951-972, 10.5194/acp-22-951-2022, 2022.

https://doi.org/10.5194/egusphere-2025-4543
Preprint. Discussion started: 30 October 2025

Vinken, G. C. M., Boersma, K. F., Jacob, D. J., and Meijer, E. W.: Accounting for non-linear chemistry of ship plumes in the GEOS-Chem global chemistry transport model, Atmospheric Chemistry and Physics, 11, 11707-11722, 10.5194/acp-11-11707-2011, 2011.

Vukicevic, T. and Errico, R. M.: LINEARIZATION AND ADJOINT OF PARAMETERIZED MOIST DIABATIC PROCESSES, Tellus Ser. A-Dyn. Meteorol. Oceanol., 45A, 493-510, 10.1034/j.1600-0870.1993.0012.x, 1993.

Wang, X. M., Carmichael, G., Chen, D. L., Tang, Y. H., and Wang, T. J.: Impacts of different emission sources on air quality during March 2001 in the Pearl River Delta (PRD) region, Atmospheric Environment, 39, 5227-5241, 10.1016/j.atmosenv.2005.04.035, 2005.

Wang, Y., Zhang, Y., Hao, J., and Luo, M.: Seasonal and spatial variability of surface ozone over China: contributions from background and domestic pollution, Atmospheric Chemistry and Physics, 11, 3511-3525, 10.5194/acp-11-3511-2011, 2011.

Wang, Y., Yaluk, E. A., Chen, H., Jiang, S., Huang, L., Zhu, A., Xiao, S., Xue, J., Lu, G., Bian, J., Kasemsan, M., Zhang, K., Liu, H., Tong, H., Ooi, M. C. G., Chan, A., and Li, L.: The Importance of NOx Control for Peak Ozone Mitigation Based on a Sensitivity Study Using CMAQ-HDDM-3D Model During a Typical Episode Over the Yangtze River Delta Region, China, Journal of Geophysical Research: Atmospheres, 127, 10.1029/2022jd036555, 2022.

Wang, Y. H., Jacob, D. J., and Logan, J. A.: Global simulation of tropospheric O-3-NOx-hydrocarbon chemistry 1. Model formulation, Journal of Geophysical Research: Atmospheres, 103, 10713-10725, 10.1029/98JD00158, 1998.

Wesely, M. L.: Parameterization of surface resistances to gaseous dry deposition in regional-scale numerical models, Atmospheric Environment (1967), 23, 1293-1304, https://doi.org/10.1016/0004-6981(89)90153-4, 1989.

Whaley, C. H., Strong, K., Jones, D. B. A., Walker, T. W., Jiang, Z., Henze, D. K., Cooke, M. A., McLinden, C. A., Mittermeier, R. L., Pommier, M., and Fogal, P. F.: Toronto area ozone: Long-term measurements and modeled sources of poor air quality events, Journal of Geophysical Research-Atmospheres, 120, 11368-11390, 10.1002/2014jd022984, 2015.

Yan, Y. Y., Cabrera-Perez, D., Lin, J. T., Pozzer, A., Hu, L., Millet, D. B., Porter, W. C., and Lelieveld, J.: Global tropospheric effects of aromatic chemistry with the SAPRC-11 mechanism implemented in GEOS-Chem version 9-02, Geoscientific Model Development, 12, 111-130, 10.5194/gmd-12-111-2019, 2019.

Yang, J. Y. and Zhao, Y.: Performance and application of air quality models on ozone simulation in China - A review, Atmospheric Environment, 293, 20, 10.1016/j.atmosenv.2022.119446, 2023.

Zhang, L., Shao, J. Y., Lu, X., Zhao, Y. H., Hu, Y. Y., Henze, D. K., Liao, H., Gong, S. L., and Zhang, Q.: Sources and Processes Affecting Fine Particulate Matter Pollution over North China: An Adjoint Analysis of the Beijing APEC Period, Environmental Science & Technology, 50, 8731-8740, 10.1021/acs.est.6b03010, 2016.

Zhang, W., Capps, S. L., Hu, Y., Nenes, A., Napelenok, S. L., and Russell, A. G.: Development of the high-order decoupled direct method in three dimensions for particulate matter: enabling advanced sensitivity analysis in air quality models, Geoscientific Model Development, 5, 355-368, 10.5194/gmd-5-355-2012, 2012.

Zhang, Y., Tang, L., Sun, Y., Favez, O., Canonaco, F., Albinet, A., Couvidat, F., Liu, D., Jayne, J. T., Wang, Z., Croteau, P. L., Canagaratna, M. R., Zhou, H.-c., Prévôt, A. S. H., and Worsnop, D. R.: Limited formation of isoprene epoxydiols-derived secondary organic aerosol under NOx-rich environments in Eastern China, Geophysical Research Letters, 44, 2035-2043, https://doi.org/10.1002/2016GL072368, 2017.

Zhang, Y. Z., Gautam, R., Pandey, S., Omara, M., Maasakkers, J. D., Sadavarte, P., Lyon, D., Nesser, H., Sulprizio, M. P., Varon, D. J., Zhang, R. X., Houweling, S., Zavala-Araiza, D., Alvarez, R. A., Lorente, A., Hamburg, S. P., Aben, I., and Jacob, D. J.: Quantifying methane emissions from the largest oil-producing basin in the United States from space, Sci. Adv., 6, 9, 10.1126/sciadv.aaz5120, 2020.

Zhao, Y. S., Li, Y. T., Kumar, A., Ying, Q., Vandenberghe, F., and Kleeman, M. J.: Separately resolving NOx and VOC contributions to ozone formation, Atmospheric Environment, 285, 15, 10.1016/j.atmosenv.2022.119224, 2022.

Zhu, L., Henze, D., Bash, J., Jeong, G. R., Cady-Pereira, K., Shephard, M., Luo, M., Paulot, F., and Capps, S.: Global evaluation of ammonia bidirectional exchange and livestock diurnal variation schemes, Atmospheric Chemistry and Physics, 15, 12823-12843, 10.5194/acp-15-12823-2015, 2015.